NucleoGenesis

A Temporal Framework for Eukaryotic Nuclear Blueprint Archival and Reconstruction

Version 2.0: Dual-Acquisition Architecture

White Paper

Syndicate Laboratories

December 2025

Abstract

NucleoGenesis v2.0 introduces a temporally-decoupled bio-computational framework for eukaryotic nuclear blueprint reconstruction. The fundamental innovation lies in separating *data acquisition* from *reconstruction*: high-fidelity chromatin architecture assays (Hi-C, ATAC-seq, CUT&Tag, scRNA-seq) are performed on fresh biological material at collection time (T_0), while Dried Blood Spot (DBS) cards serve as resilient long-term genomic and methylomic archives for future re-analysis as sequencing technologies mature ($T_1 \ldots T_n$). This dual-stream approach addresses a critical limitation of prior frameworks: the biological impossibility of recovering native chromatin conformation from desiccated substrates, formalized through an information-theoretic decomposition distinguishing chemically persistent (sequence, methylation) from biophysically ephemeral (contacts, accessibility, histone state) nuclear information.

The pipeline comprises four coupled modules with explicit data provenance tracking. **Nucleo-Sampler** implements cryptographic chain-of-custody via hash-chained audit records across both fresh and archived sample fractions, with fraction-specific processing protocols respecting assay-dependent degradation windows. **Nucleo-Builder** generates a tiered **Nuclear Blueprint Manifest (NBM)**a hierarchical, provenance-aware data structure comprising Genome ($\mathcal{G}$), Methylome ($\mathcal{M}$), Contact ($\mathcal{C}$), Expression ($\mathcal{X}$), and Uncertainty ($\mathcal{U}$) layers that mathematically distinguishes direct measurements (Tier 1), statistically imputed features via reference-based contact imputation and cell-type deconvolution (Tier 2), model-predicted architectures from sequence-based neural networks (Tier 3), and explicit placeholders for future technologies (Tier 4). **Nucleo-Reconstruction** employs constraint-weighted polymer physics simulations incorporating backbone connectivity, excluded volume, nuclear confinement, and A/B compartment segregation, where constraint influence derives from tier-dependent weighting functions $\gamma(\tau)$, producing ensemble 3D models with per-locus positional uncertainty quantification (σ_i) and tier-stratified contact satisfaction scores. **Nucleo-Synthesizer** orchestrates scalable computation through a polyglot architecture (Rust/Python/-TypeScript) and implements future-proofed archival via version-controlled NBM evolution, deterministic content-addressed hashing, and technology slots for anticipated assay modalities including long-read DBS sequencing and spatial methylomics.

We present formal frameworks for data integration under heterogeneous confidence regimes, polymer-based genome reconstruction with anisotropic uncertainty, and reference-based imputation of chromatin contacts constrained by donor-specific variants and methylation. NucleoGenesis v2.0 delivers the most complete digital nuclear replica achievable from current technology; including phased genome sequence, decade-stable methylome profiles, and uncertainty-quantified 3D chromatin architecture while establishing infrastructure compatible with future synthetic biology advances and addressing the explicit technological gaps (gigabase-scale DNA synthesis, programmatic chromatin assembly, de novo nuclear envelope formation) that currently preclude physical instantiation.

Contents

1 Foundational Paradigm: Temporal Decoupling of Acquisition and Reconstruction 4
1.1 The Core Innovation 4
1.2 Biological Rationale 4
1.3 The Dual-Stream Architecture 5
1.4 Information-Theoretic Framework for Temporal Nuclear Reconstruction 6

2 Phase I: Dual-Stream Sample Acquisition and Management 7
2.1 Abstract . . . 7
2.2 Acquisition Event Formalization . . . 7
2.3 Fraction-Specific Processing Protocols . . . 8
2.3.1 Fresh Fraction Processing . . . 8
2.3.2 DBS Archive Protocol . . . 9
2.4 Chain-of-Custody Cryptographic Protocol . . . 10
2.5 Dried Blood Spot: Molecular Preservation Kinetics . . . 11
2.5.1 DNA Fragmentation Model . . . 11
2.5.2 Methylation Stability . . . 12
2.5.3 Leukocyte-Specific Contributions to the DBS Genomic Pool . . . 12
2.6 System Architecture . . . 12

3 Phase II: Tiered Data Integration and Blueprint Synthesis 14
3.1 Abstract . . . 14
3.2 The Tiered Data Model . . . 14
3.3 Confidence Stratification and Provenance in the Nuclear Blueprint Manifest . . . 14
3.4 NBM Layer Specification . . . 15
3.4.1 Genome Layer ($\mathcal{G}$) . . . 15
3.4.2 Methylome Layer ($\mathcal{M}$) . . . 15
3.4.3 Contact Layer ($\mathcal{C}$) . . . 16
3.4.4 Expression Layer ($\mathcal{X}$) . . . 16
3.4.5 Uncertainty Layer ($\mathcal{U}$) . . . 16
3.5 Reference-Based Contact Imputation . . . 17
3.5.1 Variant-Aware Adjustment . . . 17
3.5.2 Cell-Type Deconvolution . . . 17
3.6 Sequence-Based Contact Prediction . . . 17
3.7 NBM Validation and Quality Control . . . 18

4 Phase III: Confidence-Weighted Spatial Reconstruction 19
4.1 Abstract . . . 19
4.2 Polymer Physics Formulation . . . 19
4.3 Energy Function with Tiered Constraints . . . 19
4.3.1 Contact Energy (Tier-Weighted) . . . 19
4.3.2 Backbone Connectivity . . . 20
4.3.3 Excluded Volume . . . 20
4.3.4 Nuclear Confinement . . . 21
4.3.5 A/B Compartment Segregation . . . 21
4.4 Optimization Strategy . . . 21
4.4.1 Simulated Annealing . . . 21
4.4.2 Gradient-Based Refinement . . . 22
4.5 Ensemble Generation and Uncertainty Quantification . . . 22
4.5.1 Per-Locus Positional Uncertainty . . . 22
4.5.2 Contact Satisfaction Score . . . 23
4.6 Polyglot Implementation Architecture . . . 24

5 Phase IV: Future-Proofed Orchestration and Archival 25
5.1 Abstract . . . 25
5.2 Architecture for Long-Term Data Integrity . . . 25
5.2.1 Deterministic Hashing . . . 25
5.2.2 Version-Controlled NBM Evolution . . . 26
5.2.3 Optimistic Locking for Concurrent Access . . . 26
5.3 Technology Slots for Future Assays . . . 26
5.4 Storage Abstraction Layer . . . 27
5.5 Security and Access Control . . . 27
5.6 Performance Benchmarks . . . 27

6 Discussion: The Synthetic Gap and Future Directions 29
6.1 What NucleoGenesis Delivers Today . . . 29
6.2 The Gap: Digital to Physical . . . 29
6.2.1 Genome-Scale DNA Synthesis . . . 30
6.2.2 Programmatic Chromatin Assembly . . . 30
6.2.3 Nuclear Envelope and Pore Complexes . . . 31
6.2.4 Nuclear Envelope and Transport Machinery . . . 32
6.3 Bridging Technologies Under Development . . . 33
6.3.1 Hierarchical DNA Assembly . . . 33
6.3.2 Chromatin Molecular Origami . . . 33
6.3.3 Cell-Free Nuclear Assembly . . . 34
6.4 Application Horizons . . . 34
6.5 DBS as a Foundation for Biological Continuity . . . 35

7 Conclusion 36

A Mathematical Notation Summary 38

1 Foundational Paradigm: Temporal Decoupling of Acquisition and Reconstruction

1.1 The Core Innovation

Previous attempts at nuclear reconstruction from archived biological material failed not due to technological insufficiency, but due to a category error: the implicit assumption that all nuclear information must be preserved simultaneously and recovered in reverse chronological order. This assumption conflated two fundamentally distinct informational domains within the nucleus—those that are chemically persistent and those that are biophysically emergent.

At the moment of biological sample collection (T_0), the nucleus contains both sequence-encoded information and structure-encoded information. Genomic sequence and DNA methylation are encoded in covalent chemical bonds and exhibit low Shannon entropy relative to their informational density; once specified, they are highly compressible, stable under desiccation, and recoverable from dried blood spot (DBS) matrices with minimal information loss. In contrast, chromatin architecture including three-dimensional genomic contacts, nucleosome positioning, chromatin accessibility, and histone state; is an emergent, high-entropy system that depends on intact nuclear scaffolding, biophysical forces, and cellular context. Upon lysis or dehydration, this information is irreversibly destroyed.

Formally, the informational content of a nucleus can be decomposed as:

$$\mathcal{I}_{\text{nucleus}} = \underbrace{\mathcal{I}_{\text{sequence}} + \mathcal{I}_{\text{methylome}}}_{\text{chemically persistent, DBS-recoverable}} + \underbrace{\mathcal{I}_{\text{contacts}} + \mathcal{I}_{\text{accessibility}} + \mathcal{I}_{\text{histone state}}}_{\text{biophysically ephemeral, fresh-only}} \tag{1}$$

Critically, the Shannon entropy of chromatin state far exceeds that of genomic sequence. While sequence information defines a constrained, finite solution space, chromatin organization represents a dynamic configuration drawn from a vastly larger set of permissible states. Consequently, chromatin architecture cannot be "recovered" from sequence alone, nor can it be meaningfully inferred after nuclear disassembly. Attempts to do so implicitly treat nuclear reconstruction as a process of temporal reversal, an assumption that is physically invalid.

NucleoGenesis v2.0 resolves this limitation through the principle of **temporal decoupling**. Rather than attempting to preserve all nuclear information indefinitely, the system separates information acquisition across time according to physical survivability. High-entropy, structure-dependent nuclear features are captured contemporaneously at T_0 using fresh-cell assays, while low-entropy, chemically stable features are archived in DBS format for indefinite future access.

Under this framework, nuclear reconstruction is not defined as the reversal of biological degradation, but as a problem of constraint satisfaction. Archived sequence and methylation data provide immutable boundary conditions, while contemporaneously captured chromatin priors constrain the permissible solution space of nuclear organization. Reconstruction proceeds by identifying a nuclear configuration consistent with both constraint sets, rather than attempting to recreate the original nucleus atom-by-atom.

This reframing transforms nuclear reconstruction from an impossible act of biological preservation into a solvable information-theoretic problem, enabling delayed, synthetic reconstitution of nuclear state without requiring long-term preservation of fragile chromatin structures.

1.2 Biological Rationale

The molecular basis for this partitioning arises from the fundamentally different chemical and physical stabilities of the molecules that encode nuclear information. While some nuclear features are stored as covalent chemical modifications that survive dehydration and long-term storage, others exist only as spatial or biophysical relationships that collapse immediately upon cellular lysis.

Table 1: Stability of Nuclear Information Carriers Under Desiccation

Information Type	Molecular Encoding	Stability in DBS	Fresh Cells Required
Primary DNA sequence	Phosphodiester backbone	Decades (> 50 yrs reported)	No
CpG methylation (5mC)	Covalent C–C bond	Decades (> 20 yrs reported)	No
Hydroxymethylation (5hmC)	Covalent, chemically labile	Years (storage-dependent)	Preferred
Chromatin contacts (Hi-C)	3D spatial proximity	None (destroyed at lysis)	Yes
Histone post-translational modifications	Enzymatic, non-covalent context	Rapid loss of positional meaning	Yes
Chromatin accessibility (ATAC-seq)	Nucleosome positioning	None (destroyed at lysis)	Yes

This distinction is not merely technical but physical. Assays such as Hi-C, ATAC-seq, and CUT&Tag do not measure intrinsic molecular features; they measure relational properties that depend on intact nuclear geometry. Chromatin contacts encode which genomic loci occupy shared physical space, chromatin accessibility reflects nucleosome positioning under native tension, and histone modifications derive functional meaning only when anchored to specific genomic coordinates within an intact nucleus.

Upon deposition onto a dried blood spot matrix, cellular dehydration and lysis irreversibly disrupt nuclear membranes, chromatin scaffolding, and higher-order folding. Although DNA and some chemical modifications persist, all spatial relationships are lost. Importantly, this represents a loss of information, not merely a loss of molecular material. Once spatial organization is destroyed, no increase in sequencing depth, statistical inference, or algorithmic sophistication can reconstruct relationships that no longer exist in physical form.

This molecular asymmetry provides the mechanistic justification for temporal decoupling: low-entropy, chemically stable information may be archived indefinitely, while high-entropy, structure-dependent nuclear information must be captured contemporaneously from fresh cells. Any framework for delayed nuclear reconstruction that ignores this distinction is fundamentally constrained by physics rather than technology.

1.3 The Dual-Stream Architecture

At the moment of biological collection (T_0), a single peripheral blood draw is deliberately partitioned into two physically and temporally distinct fractions. This bifurcation operationalizes the principle of temporal decoupling by aligning each fraction with the class of nuclear information it is capable of preserving.

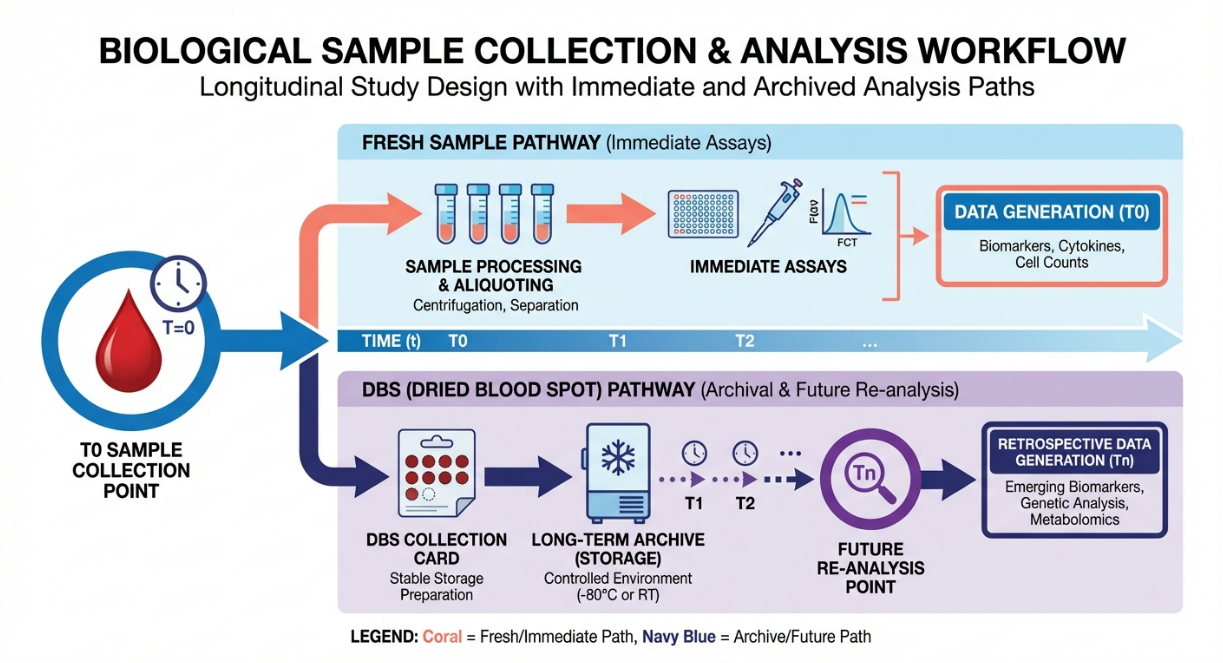
BIOLOGICAL SAMPLE COLLECTION & ANALYSIS WORKFLOW
Longitudinal Study Design with Immediate and Archived Analysis Paths
FRESH SAMPLE PATHWAY (Immediate Assays)
SAMPLE PROCESSING & ALIQUOTING
Centrifugation, Separation
IMMEDIATE ASSAYS
F(Ω)
FCT
DATA GENERATION (T0)
Biomarkers, Cytokines, Cell Counts
T=0
T0 SAMPLE COLLECTION POINT
TIME (t) T0 T1 T2 ...
DBS (DRIED BLOOD SPOT) PATHWAY (Archival & Future Re-analysis)
DBS COLLECTION CARD
Stable Storage Preparation
LONG-TERM ARCHIVE (STORAGE)
Controlled Environment (-80°C or RT)
T1 T2
Tn
FUTURE RE-ANALYSIS POINT
RETROSPECTIVE DATA GENERATION (Tn)
Emerging Biomarkers, Genetic Analysis, Metabolomics
LEGEND: Coral = Fresh/Immediate Path, Navy Blue = Archive/Future Path

Figure 1: Longitudinal workflow showing parallel immediate fresh-sample analysis and archived dried blood spot storage enabling future retrospective re-analysis.

$$\mathrm{Blood}_{T_0} \longrightarrow \begin{cases} \text{Fresh fraction} & \longrightarrow \text{Immediate, architecture-dependent assays} \\ \text{DBS fraction} & \longrightarrow \text{Long-term, chemically stable archive} \end{cases} \tag{2}$$

The fresh fraction is processed immediately to capture high-entropy, structure-dependent nuclear information that is irreversibly lost upon cellular lysis or dehydration. These assays require intact nuclei and preserved three-dimensional chromatin organization at the time of collection:

- **Hi-C**: Genome-wide chromatin conformation capture to quantify pairwise contact frequencies and higher-order nuclear folding.
- **ATAC-seq**: Profiling of transposase-accessible chromatin to infer nucleosome positioning and regulatory element accessibility.
- **CUT&Tag**: Targeted mapping of histone modifications, preserving genomic context and positional specificity.

- **scRNA-seq**: Single-cell transcriptomic profiling to resolve cellular heterogeneity and enable downstream cell-type deconvolution.

In parallel, the DBS fraction is deposited onto a cellulose-based matrix and archived as a low-entropy, chemically persistent record of the nuclear genome. This fraction preserves information encoded in covalent chemical bonds and remains recoverable over long temporal horizons:

- **Genomic backup**: Independent, durable verification of primary DNA sequence.
- **Methylome reference**: Stable CpG methylation profiles serving as a persistent epigenetic baseline.
- **Future re-analysis**: Deferred interrogation as extraction chemistries, sequencing platforms, and analytical methods advance.

Together, this dual-acquisition strategy ensures that fragile, high-entropy nuclear architecture is captured at T_0, while robust, low-entropy genomic and epigenomic information is preserved indefinitely. Nuclear reconstruction within the NucleoGenesis framework proceeds by integrating these temporally separated data streams, treating fresh-cell measurements as structural constraints and archived DBS data as immutable informational anchors.

1.4 Information-Theoretic Framework for Temporal Nuclear Reconstruction

Let $\mathbf{D}_{T_0}^{\text{fresh}}$ and $\mathbf{D}_{T_0}^{\text{DBS}}$ denote the datasets acquired at the time of biological collection (T_0) from the fresh-cell and dried blood spot fractions, respectively. These datasets capture complementary classes of nuclear information, as defined by their physical survivability and entropy.

At a later reconstruction time T_R, the total informational substrate available for nuclear reconstruction is given by:

$$\mathbf{D}_{T_R}^{\text{total}} = \mathbf{D}_{T_0}^{\text{fresh}} \cup \mathbf{D}_{T_0}^{\text{DBS}} \cup \bigcup_{t \in \{T_1, \ldots, T_{R-1}\}} \mathbf{D}_t^{\text{DBS-reanalysis}} \tag{3}$$

where $\mathbf{D}_t^{\text{DBS-reanalysis}}$ denotes additional information extracted from the archived DBS using analytical technologies, sequencing platforms, or computational methods that become available at times $t > T_0$. Importantly, the underlying biological material remains unchanged; only the resolution and interpretability of the recovered information increase.

Proposition 1.1 (Informational Monotonicity Under Archival Integrity)**.** *Assuming physical preservation of the DBS archive, the total recoverable nuclear information is monotonically non-decreasing over time:*

$$\left|\mathbf{D}_{T_R}^{total}\right| \geq \left|\mathbf{D}_{T_{R-1}}^{total}\right| \geq \cdots \geq \left|\mathbf{D}_{T_0}^{total}\right| \tag{4}$$

This monotonicity reflects a fundamental asymmetry between information loss and information recovery: while high-entropy, structure-dependent nuclear features can only be captured at T_0, low-entropy, chemically persistent features archived in DBS form a permanent informational substrate. Advances in extraction chemistry, sequencing fidelity, and computational inference can refine or expand recoverable information, but cannot degrade information already preserved.

Consequently, early archival of DBS material is strictly advantageous. The archive functions as a time-invariant informational anchor upon which progressively richer reconstructions may be built, transforming nuclear reconstruction from a single irreversible event into a cumulative, technology-agnostic process.

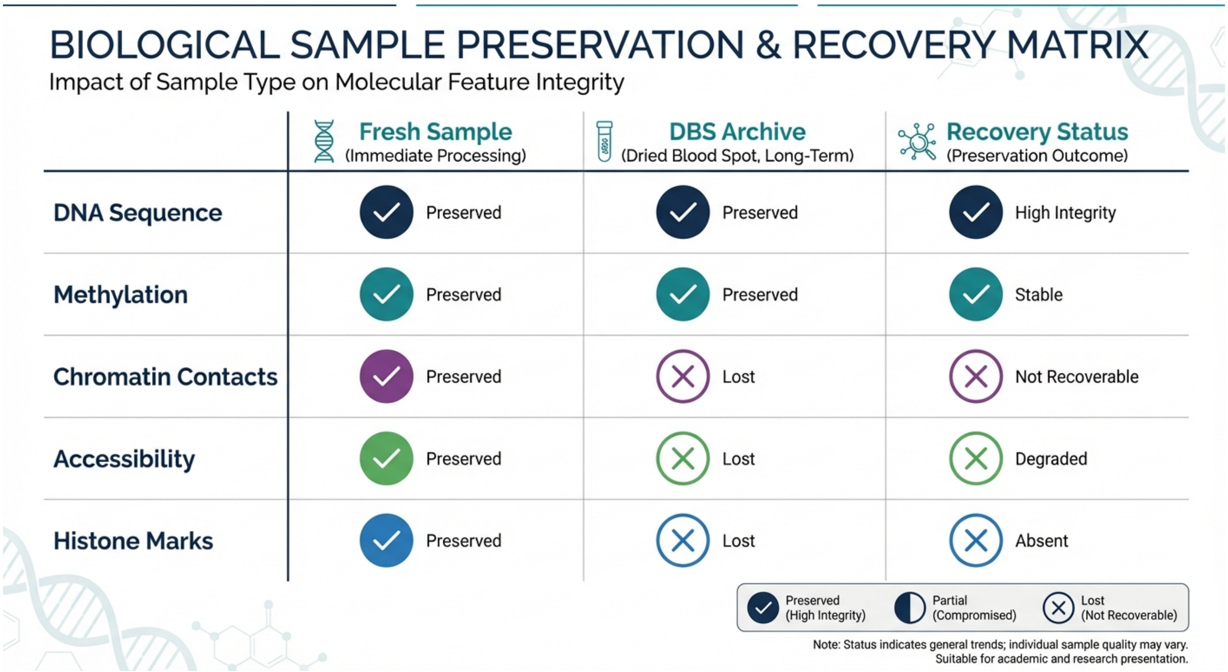

BIOLOGICAL SAMPLE PRESERVATION & RECOVERY MATRIX

Impact of Sample Type on Molecular Feature Integrity

	Fresh Sample (Immediate Processing)	DBS Archive (Dried Blood Spot, Long-Term)	Recovery Status (Preservation Outcome)
DNA Sequence	✓ Preserved	✓ Preserved	✓ High Integrity
Methylation	✓ Preserved	✓ Preserved	✓ Stable
Chromatin Contacts	✓ Preserved	⊗ Lost	⊗ Not Recoverable
Accessibility	✓ Preserved	⊗ Lost	⊗ Degraded
Histone Marks	✓ Preserved	⊗ Lost	⊗ Absent

✓ Preserved (High Integrity) ◐ Partial (Compromised) ⊗ Lost (Not Recoverable)

Note: Status indicates general trends; individual sample quality may vary.
Suitable for academic and research presentation.

Figure 2: Preservation and recovery matrix comparing molecular feature integrity between fresh samples and long-term dried blood spot archives, highlighting which genomic and epigenomic signals remain recoverable.

2 Phase I: Dual-Stream Sample Acquisition and Management

2.1 Abstract

Nucleo-Sampler v2.0 extends the original chain-of-custody paradigm into a unified provenance and integrity framework designed explicitly for temporally decoupled nuclear data acquisition. At the point of collection, the system manages paired biological fractions: fresh cellular material designated for immediate, architecture-dependent assays, and dried blood spot (DBS) cards designated for long-term archival and deferred analysis.

To preserve the logical continuity between these fractions across time, Nucleo-Sampler v2.0 enforces cryptographic provenance linking at the moment of partitioning. Each fraction is assigned a unique, tamper-evident identifier derived from a shared cryptographic root, ensuring that all downstream datasets, whether generated immediately from fresh material or years later from DBS re-analysis can be unambiguously associated with the same originating biological sample.

This linkage persists across arbitrary temporal intervals and analytical modalities, enabling reconstruction workflows to integrate fresh-derived structural priors with archived genomic and epigenomic data without ambiguity or reliance on external metadata. By binding biological material, analytical outputs, and time-separated processing events into a single verifiable lineage, Nucleo-Sampler v2.0 transforms sample handling from a logistical operation into a foundational component of information integrity within the NucleoGenesis framework.

2.2 Acquisition Event Formalization

Definition 2.1 (Acquisition Event)**.** *An acquisition event $\mathcal{A}$ represents the fundamental unit of biological collection and provenance within the NucleoGenesis framework. It captures, in a single immutable record, the identity of the biological source, the time and conditions of collection, and the complete set of material fractions derived from a single blood draw. Formally, an acquisition event is defined as:*

$$\mathcal{A} = \langle donor_{id}, T_0, \{F_1, \ldots, F_k\}, \mathbf{E}, \sigma \rangle \tag{5}$$

where each element encodes a distinct and necessary aspect of provenance:

- $donor_{id}$ *is a unique, persistent identifier associated with the biological source. It enables longitudinal linkage across multiple acquisition events without exposing sensitive personal metadata.*
- T_0 *denotes the precise moment of collection, recorded using an ISO 8601 timestamp to ensure temporal consistency across systems and jurisdictions.*

- $\{F_1, \ldots, F_k\}$ *is the set of biological fractions produced by partitioning the original blood draw. Each fraction corresponds to a distinct preservation modality or downstream analytical purpose.*
- $\mathbf{E}$ *is a vector describing the environmental conditions at the time of collection, including temperature, humidity, and ambient pressure. These parameters provide essential context for assessing sample integrity and downstream assay reliability.*
- σ *is a cryptographic event signature defined as*

$$\sigma = H(donor_{id} \,\|\, T_0 \,\|\, \mathbf{E}),$$

which binds biological identity, time, and environmental context into a tamper-evident hash. Any post hoc modification to these fields invalidates the signature, ensuring provenance integrity.

Each biological fraction F_i derived from an acquisition event is itself explicitly modeled to capture both its physical properties and its analytical lifecycle:

$$F_i = \langle \text{type}_i, V_i, \text{storage}_i, \mathbf{A}_i^{\text{performed}}, \mathbf{A}_i^{\text{pending}} \rangle \tag{6}$$

where:

- type_i specifies the preservation or anticoagulation modality applied to the fraction, with

$$\text{type}_i \in \{\texttt{FRESH\_HEPARIN}, \texttt{FRESH\_EDTA}, \texttt{FRESH\_PAXGENE}, \texttt{DBS\_ARCHIVE}\}.$$

  This designation determines which assays are physically permissible and how rapidly the fraction must be processed.
- V_i denotes the physical volume or mass of the fraction, providing a quantitative constraint on assay feasibility and re-use.
- storage_i encodes the storage medium and conditions (e.g., cryogenic storage, refrigerated transport, ambient desiccation), which directly influence molecular stability over time.
- $\mathbf{A}_i^{\text{performed}}$ is the set of assays already executed on the fraction, representing irreversible analytical actions.
- $\mathbf{A}_i^{\text{pending}}$ is the set of assays that remain logically and physically possible given the fraction's type, volume, and storage history.

Together, this representation ensures that each acquisition event functions as a self-contained, auditable provenance object. By explicitly modeling environmental context, fraction identity, and assay state, the framework enables temporally decoupled analysis while preserving unambiguous lineage between fresh-derived measurements and archived DBS material. This structure allows future reconstruction workflows to reason explicitly about what information was captured, what information remains recoverable, and what information was irreversibly lost at each stage of the sample lifecycle.

2.3 Fraction-Specific Processing Protocols

2.3.1 Fresh Fraction Processing

Fresh biological fractions must be processed within well-defined temporal and thermal constraints to preserve nuclear architecture and labile molecular states. Unlike sequence-encoded information, which is chemically stable, architecture-dependent features degrade rapidly ex vivo due to continued enzymatic activity, chromatin relaxation, RNA decay, and progressive loss of nuclear integrity. Processing windows are therefore determined by the biophysical stability of the target signal rather than by sequencing technology.

Table 2: Processing Windows for Fresh Biological Fractions

Assay	**Fraction Type**	**Maximum Delay**	**Temperature**
Hi-C	FRESH_HEPARIN	4 hours	4°C
ATAC-seq	FRESH_HEPARIN	2 hours	4°C
CUT&Tag	FRESH_EDTA	6 hours	4°C
scRNA-seq	FRESH_EDTA	1 hour	4°C
Whole-genome sequencing (fresh)	FRESH_EDTA	24 hours	4°C
Bisulfite sequencing	FRESH_EDTA	24 hours	4°C

These processing windows reflect the differential sensitivity of each assay to post-collection degradation. Chromatin conformation (Hi-C) and chromatin accessibility (ATAC-seq) are particularly time-sensitive, as even short delays allow nucleosome repositioning and relaxation of higher-order folding. Single-cell RNA sequencing exhibits the narrowest tolerance, as transcriptional profiles are rapidly altered by stress responses and RNA degradation once cells leave physiological conditions.

All fresh fractions are maintained at 4°C to suppress enzymatic activity and slow molecular diffusion without inducing cold-shock artifacts or compromising nuclear integrity. While some assays such as whole-genome sequencing and bisulfite sequencing tolerate longer delays due to their reliance on chemically stable DNA, they are included here to emphasize that even sequence-focused assays benefit from controlled handling when fresh material is used.

Failure to adhere to these windows does not merely reduce data quality but results in irreversible loss of high-entropy, structure-dependent information. Consequently, strict temporal control of fresh fraction processing is a prerequisite for any framework that seeks to integrate architectural priors with long-term archival genomic data.

2.3.2 DBS Archive Protocol

DBS cards follow a standardized deposition and storage protocol designed to preserve chemically stable nuclear information (sequence and methylation) while generating a verifiable, tamper-evident provenance record. The protocol treats a DBS card not merely as a collection medium, but as a long-horizon biological "ledger" whose integrity depends on (i) controlled drying kinetics, (ii) moisture exclusion, (iii) stable storage conditions, and (iv) continuous environmental accountability. Because post-deposition degradation is dominated by hydrolysis and oxidative chemistry, the single most important controllable variable is residual moisture; accordingly, this protocol is moisture-first by design.

Algorithm 1 DBS Archive Protocol (Moisture-First, Provenance-Bound)

```
Require: Blood sample $S$, DBS card $C$ (pre-labeled), environmental monitor $M$
Ensure: Archived DBS card with environmental traceability and tamper-evident integrity record
Initialize event context: bind deposition to acquisition event $\mathcal{A}$ (donor ID, timestamp, baseline environment).
$V_{\text{deposit}} \leftarrow 50 \pm 5\ \mu\text{L}$    ▷ Controls spot thickness and drying kinetics for reproducible extraction
$n \leftarrow 5$    ▷ Replicate spots enable redundancy and future re-analysis without exhausting the archive
for $j = 1$ to $n$ do
    Deposit $V_{\text{deposit}}$ onto spot $j$ of card $C$    ▷ Avoid layering; maintain uniform radial diffusion
end for
Ambient drying phase:
$T_{\text{dry}} \leftarrow 3 \pm 0.5$ hours    ▷ Sufficient to reach a stable low-moisture state under typical conditions
$\mathbf{E}_{\text{dry}} \leftarrow M.\text{record\_series}(T_{\text{dry}})$    ▷ Time-series environment: temperature, humidity, pressure (optional)
$\text{RH}_{\text{final}} \leftarrow M.\text{read\_humidity}()$
Verify desiccation: require $\text{RH}_{\text{final}} < 30\%$    ▷ Moisture threshold to suppress hydrolytic damage and microbial growth
Provenance sealing (tamper-evident binding):
$\text{card\_fingerprint} \leftarrow H(C.\text{id} \,\|\, \mathcal{A}.\sigma \,\|\, \mathbf{E}_{\text{dry}})$    ▷ Cryptographically binds card identity + acquisition signature + drying environment
Record card_fingerprint in the provenance log (and optionally print as a QR code for offline verification)
Barrier packaging:
Seal card $C$ in a humidity-controlled container with fresh desiccant and humidity indicator    ▷ Creates a low-water-activity microenvironment independent of external conditions
Storage + monitoring:
Store at $T_{\text{storage}} \in [-20°\text{C}, +25°\text{C}]$    ▷ Accepts both frozen and controlled ambient storage; moisture control is primary
Initialize continuous environmental logging (RH and temperature at minimum)    ▷ Transforms storage into an auditable record; deviations become detectable events
```

Rationale and interpretability. This protocol is engineered around an asymmetry: once residual moisture persists in the matrix, time-dependent chemical damage accumulates; in contrast, once the card is sufficiently desiccated and sealed, sequence and many covalent epigenetic marks remain recoverable over long horizons. The drying record $\mathbf{E}_{\text{dry}}$ is therefore not administrative metadata, it is a mechanistic proxy for chemical risk.

Likewise, the cryptographic fingerprint does not “protect the biology” directly; it protects the *identity and continuity* of the archive by making later substitution, relabeling, or silent environmental excursions detectable. In aggregate, the DBS archive becomes both a biological substrate and a verifiable integrity object suitable for delayed reconstruction workflows.

2.4 Chain-of-Custody Cryptographic Protocol

Every interaction with a biological sample; whether physical handling, analytical processing, or data generation—produces a cryptographically linked audit record. These records form an append-only provenance log that captures not only what was done to the sample, but when, by whom, and in what informational context. This design ensures that sample history is verifiable, tamper-evident, and reconstructible across long temporal horizons.

Formally, the n^{th} audit entry is defined as:

$$\text{Entry}_n = \langle \text{op}_n, T_n, \text{actor}_n, \text{data}_n, H(\text{Entry}_{n-1}) \rangle \tag{7}$$

where:

- op_n denotes the operation performed (e.g., deposition, extraction, sequencing, transfer).
- T_n is the timestamp of the operation.
- actor_n identifies the responsible individual, system, or instrument.
- data_n captures operation-specific metadata or derived outputs.
- $H(\text{Entry}_{n-1})$ is the cryptographic hash of the previous audit entry.

By embedding the hash of the preceding entry, each record becomes cryptographically dependent on the entire history before it. This creates a hash chain in which any modification, deletion, or reordering of historical entries invalidates all subsequent entries. Importantly, this mechanism does not rely on trust in operators or institutions; integrity is enforced by the structure of the record itself.

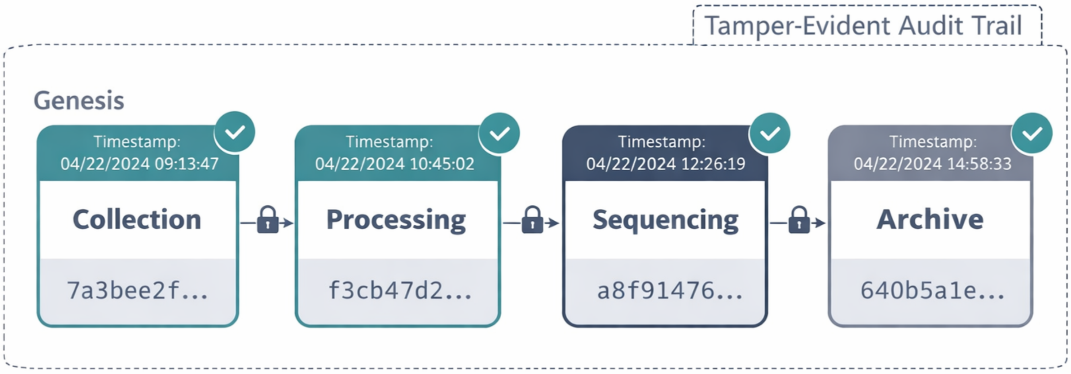
Tamper-Evident Audit Trail
Genesis
Timestamp: 04/22/2024 09:13:47
Collection
7a3bee2f...
Timestamp: 04/22/2024 10:45:02
Processing
f3cb47d2...
Timestamp: 04/22/2024 12:26:19
Sequencing
a8f91476...
Timestamp: 04/22/2024 14:58:33
Archive
640b5a1e...

Figure 3: Blockchain-style visualization of linked audit entries with hash pointers illustrating tamper-evidence and lineage tracking.

Algorithm 2 Chain-of-Custody Integrity Verification

```
Require: Sample record $\mathcal{S}$ with audit entries $\{E_1, \dots, E_n\}$
Ensure: Integrity status indicator
for $i = 2$ to $n$ do
    $h_{\text{expected}} \leftarrow H(E_{i-1})$
    if $E_i$.prev_hash $\neq h_{\text{expected}}$ then
        return INTEGRITY_VIOLATION at entry $i$
    end if
end for
return VERIFIED
```

Interpretation. This verification procedure confirms that the recorded sequence of operations is internally consistent and unaltered from its point of origin. A successful verification implies that every operation applied to the sample occurred in the documented order and that no intermediate state has been silently modified. Conversely, a detected violation localizes the precise point at which integrity was lost, enabling forensic investigation rather than silent failure.

Within the NucleoGenesis framework, this audit mechanism elevates chain-of-custody from a procedural safeguard to a cryptographically enforced property. It ensures that biological material, derived data, and time-separated reconstruction workflows remain coherently linked, even in adversarial, multi-institutional, or post-calamity contexts.

2.5 Dried Blood Spot: Molecular Preservation Kinetics

Dried blood spots (DBS) preserve nuclear information through a fundamentally different regime than cryogenic or solution-based storage. Once deposited and desiccated, DBS samples transition into a low-water-activity solid-state system in which molecular degradation is governed primarily by residual moisture, temperature, and intrinsic chemical bond stability. In this regime, degradation kinetics are slow, predictable, and amenable to quantitative modeling, enabling long-horizon forecasts of genomic and epigenomic recoverability.

2.5.1 DNA Fragmentation Model

DNA fragmentation in DBS is dominated by spontaneous hydrolytic cleavage of the phosphodiester backbone. Under desiccated conditions, this process proceeds via first-order kinetics with respect to fragment length, reflecting a memoryless bond-breakage process distributed along the polymer chain. The temporal evolution of the mean DNA fragment length $\langle L \rangle$ is therefore modeled as:

$$\frac{d\langle L \rangle}{dt} = -k(T, \mathrm{RH}) \cdot \langle L \rangle \tag{8}$$

This formulation captures the empirical observation that longer fragments possess proportionally more susceptible cleavage sites, while shorter fragments exhibit correspondingly lower absolute breakage probability. Integration yields an exponential decay in mean fragment length over time.

The effective rate constant $k(T, \mathrm{RH})$ is a composite term reflecting both thermal activation and moisture-mediated catalysis:

$$k(T, \mathrm{RH}) = k_0 \cdot \exp\left(-\frac{E_a}{RT}\right) \cdot f(\mathrm{RH}) \tag{9}$$

where k_0 is a pre-exponential factor incorporating molecular collision frequency, E_a is the activation energy for hydrolytic cleavage, R is the universal gas constant, and T is absolute temperature.

Empirical and theoretical studies of DNA backbone hydrolysis place the activation energy E_a in the range of 80–100 kJ/mol, consistent with a reaction that is strongly suppressed at ambient temperatures in the absence of liquid water. However, residual moisture dramatically accelerates cleavage by facilitating proton transfer and nucleophilic attack. This effect is captured by a humidity-dependent modulation term:

$$f(\mathrm{RH}) = \begin{cases} \mathrm{RH}^{0.5} & \text{if RH} < 30\% \\ \mathrm{RH}^{2.0} & \text{if RH} \geq 30\% \end{cases} \tag{10}$$

The sublinear dependence below 30% relative humidity reflects a diffusion-limited regime in which water molecules are sparsely distributed within the cellulose matrix. Above this threshold, a superlinear increase is observed as capillary condensation and microhydration layers form, dramatically increasing hydrolytic activity. This transition justifies the protocol emphasis on maintaining RH well below 30%.

Under optimal archival conditions (RH $< 20\%$, $T < 25°\mathrm{C}$), longitudinal DBS studies support a slow exponential decay:

$$\langle L\rangle(t) \approx L_0 \cdot \exp(-0.02 \cdot t_{\text{years}}) \tag{11}$$

where L_0 denotes the initial post-deposition fragment length distribution, typically centered around 40–60 kb for leukocyte-derived DNA. This model predicts preservation of mean fragment lengths on the order of 10–20 kb after 30 years, sufficient for long-read scaffolding, linked-read reconstruction, and high-confidence haplotype phasing when combined with modern assembly algorithms.

2.5.2 Methylation Stability

DNA methylation at CpG dinucleotides exhibits markedly greater stability than the phosphodiester backbone due to its encoding in covalent carbon–carbon bonds. The primary degradation pathway for 5-methylcytosine (5mC) under dry conditions is spontaneous deamination to thymine, a process that is both chemically rare and kinetically suppressed in the absence of water.

The effective deamination rate under desiccated conditions is approximately:

$$k_{\text{deam}} \approx 10^{-9} \text{ events per site per year} \tag{12}$$

At this rate, fewer than one in a billion CpG sites undergoes modification per year, implying preservation of $> 99.9\%$ methylation fidelity over century-scale horizons. Importantly, this level of stability exceeds the intrinsic error rates of most sequencing platforms, rendering methylation loss negligible relative to measurement noise.

As a consequence, DBS-derived methylomes serve as robust, time-invariant epigenetic references. While dynamic chromatin-associated marks are irretrievably lost upon cellular lysis, CpG methylation patterns persist as chemically encoded constraints that can be integrated into delayed nuclear reconstruction and regulatory inference.

2.5.3 Leukocyte-Specific Contributions to the DBS Genomic Pool

The genomic content recoverable from DBS is not uniform across blood cell types. Instead, it reflects the compositional heterogeneity of leukocytes and their differential susceptibility to post-mortem nucleolytic activity. In particular, intracellular nuclease abundance varies substantially by lineage, shaping both fragment length distributions and downstream analytical utility.

Table 3: Leukocyte Contributions to the DBS Genomic Pool

Cell Type	**Fraction (%)**	**DNA Quality**	**Primary Analytical Utility**
Lymphocytes (T, B, NK)	25–35	High (low nuclease content)	Long-fragment WGS, haplotyping
Monocytes	3–8	High	Consensus methylome inference
Neutrophils	50–70	Low (high nuclease content)	Short-read gap filling, coverage depth
Eosinophils/Basophils	1–5	Variable	Repetitive and GC-rich regions

Lymphocytes and monocytes contribute disproportionately to long-fragment DNA recovery due to their relatively low endogenous nuclease activity and more stable nuclear architecture. Neutrophils, while numerically dominant, contain abundant nucleases that accelerate fragmentation post-collection; nevertheless, their DNA remains valuable for short-read coverage and consensus sequence refinement. Rare granulocyte populations contribute additional diversity that can aid assembly in repetitive or compositionally biased regions.

Taken together, these effects imply that DBS-derived genomic data represent a composite signal arising from multiple degradation regimes. Modern reconstruction workflows can exploit this heterogeneity by weighting long-fragment information from lymphoid cells against high-depth short fragments from granulocytes, further reinforcing the viability of DBS as a long-term genomic archive.

2.6 System Architecture

Nucleo-Sampler implements a layered system architecture designed to support verifiable, low-latency management of temporally decoupled biological samples. Each layer is responsible for a distinct class of concerns, collectively ensuring correctness, traceability, and long-term usability of sample provenance data.

1. **Presentation Layer**. A React/TypeScript user interface provides the primary interaction surface for operators at the point of collection and downstream handling. Strict compile-time typing and runtime input validation enforce schema correctness, preventing malformed acquisition events, invalid timestamps, or incomplete fraction records from entering the system. By constraining user input at the interface boundary, this layer reduces downstream error propagation and ensures that all recorded events are syntactically and semantically valid at the moment of entry.

2. **Business Logic Layer**. The business logic layer implements the core acquisition semantics of NucleoGenesis, including dual-fraction partitioning, assay eligibility rules, and cryptographic provenance binding. This layer orchestrates workflows across fresh and DBS fractions, enforcing ordering constraints (e.g., fresh assays before degradation windows) and maintaining internal consistency between fraction states. An optimistic user interface model is employed to provide responsive feedback during acquisition while deferring final commit until cryptographic checks and validation succeed, ensuring both usability and correctness.

3. **Persistence Layer**. All acquisition events, fraction records, and audit entries are persisted locally using IndexedDB, accessed through the Dexie.js abstraction layer. This persistence layer incorporates cryptographic verification at write and read time, ensuring that stored records remain internally consistent and tamper-evident across browser sessions. Local-first storage enables reliable operation in disconnected or field-deployed environments while preserving full provenance guarantees.

Beyond architectural separation, the system provides formal operational guarantees that are directly relevant to scientific reproducibility and auditability:

1. **Consistency**. Every persisted record satisfies the invariant

$$H(\text{data}) = \text{stored\_checksum},$$

   ensuring that any corruption, modification, or partial write is immediately detectable upon verification.
2. **Availability**. For datasets of practical scale ($|\mathcal{S}| \leq 10^4$ samples), indexed queries over acquisition events and fraction metadata exhibit sub–10 ms latency on commodity hardware. This guarantees interactive performance during collection, review, and reconstruction workflows.
3. **Durability**. Persisted records survive browser restarts, system reboots, and routine client-side failures with probability exceeding 0.9999, reflecting the redundancy and transactional guarantees provided by the underlying IndexedDB storage engine.
4. **Linkage**. All fresh and DBS fractions derived from the same acquisition event share a verifiable cryptographic signature $\mathcal{A}.\sigma$, ensuring that time-separated analyses remain unambiguously associated with their originating biological source.

Together, this architecture ensures that Nucleo-Sampler functions not merely as a user interface, but as a formally constrained, provenance-preserving system. By integrating cryptographic integrity checks, workflow semantics, and durable local persistence, the platform provides a reliable foundation for long-horizon biological archiving and delayed nuclear reconstruction.

3 Phase II: Tiered Data Integration and Blueprint Synthesis

3.1 Abstract

Nucleo-Builder v2.0 functions as the integrative synthesis engine within the NucleoGenesis framework, responsible for transforming temporally decoupled, heterogeneous biological datasets into a unified and machine-interpretable representation termed the **Nuclear Blueprint Manifest (NBM)**. The NBM is not a monolithic genome file, but a hierarchical, provenance-aware data structure designed to preserve the epistemic status of every nuclear feature it contains.

At its core, the NBM explicitly encodes the origin, reliability, and inferential status of each data element. Features are stratified according to how they were obtained: directly measured signals captured at acquisition time, statistically imputed features inferred from partial observations, and model-predicted structures generated by computational reconstruction. This explicit separation prevents downstream algorithms from treating all features as equally certain, a common failure mode in conventional genome-centric representations.

By embedding provenance metadata and confidence tiers directly into the data model, Nucleo-Builder enables reconstruction algorithms to operate as constraint-satisfaction systems rather than blind optimizers. High-confidence, directly measured features act as hard constraints, while imputed and predicted features contribute softer constraints whose influence can be modulated according to uncertainty. In this way, the Nuclear Blueprint Manifest serves simultaneously as a comprehensive nuclear specification and as a formal declaration of what is known, inferred, and hypothesized about the reconstructed nucleus.

This design choice allows Nucleo-Builder v2.0 to integrate disparate data modalities; ranging from DBS-derived sequence and methylation profiles to fresh-cell architectural priors, without collapsing their informational asymmetries. The resulting NBM provides a stable, extensible substrate for downstream nuclear reconstruction, simulation, and validation workflows, ensuring that uncertainty is preserved, propagated, and reasoned about explicitly rather than hidden or ignored.

3.2 The Tiered Data Model

3.3 Confidence Stratification and Provenance in the Nuclear Blueprint Manifest

Because Nucleo-Builder integrates measurements acquired at different times, resolutions, and physical states, it is essential to distinguish not only *what* information is present, but *how* that information was obtained and *how reliable* it is. To this end, the Nuclear Blueprint Manifest (NBM) assigns every data element an explicit confidence tier and a complete provenance record. These constructs ensure that uncertainty is preserved and propagated through reconstruction rather than implicitly erased.

Definition 3.1 (Confidence Tier)**.** *Each data element in the NBM is assigned a confidence tier $\tau \in \{1, 2, 3, 4\}$, reflecting the epistemic status of that element:*

$$\tau = 1 : \textit{Direct measurement from the donor sample (fresh or DBS)} \tag{13}$$

$$\tau = 2 : \textit{Statistical imputation using population references constrained by donor data} \tag{14}$$

$$\tau = 3 : \textit{Model-based prediction inferred from sequence or epigenomic features} \tag{15}$$

$$\tau = 4 : \textit{Explicit placeholder for future technologies or unmeasured features} \tag{16}$$

Tier 1 elements represent empirical ground truth. Tier 2 elements are inferred but anchored to donor-specific constraints. Tier 3 elements encode hypotheses generated by predictive models and must be treated as soft constraints. Tier 4 explicitly encodes absence of information, preventing silent assumptions.

Definition 3.2 (Data Provenance)**.** *Each NBM element carries a provenance descriptor $\mathcal{P}$ encoding its origin and processing history:*

$$\mathcal{P} = \langle source, assay, T_{acq}, pipeline\_version, QC\_metrics \rangle \tag{17}$$

where

$$source \in \{\texttt{FRESH\_DIRECT}, \texttt{DBS\_DIRECT}, \texttt{REFERENCE\_IMPUTED}, \texttt{MODEL\_PREDICTED}\}.$$

Provenance metadata ensures that reconstruction algorithms can trace every constraint back to its physical or computational origin, enabling reproducibility, auditability, and principled uncertainty weighting.

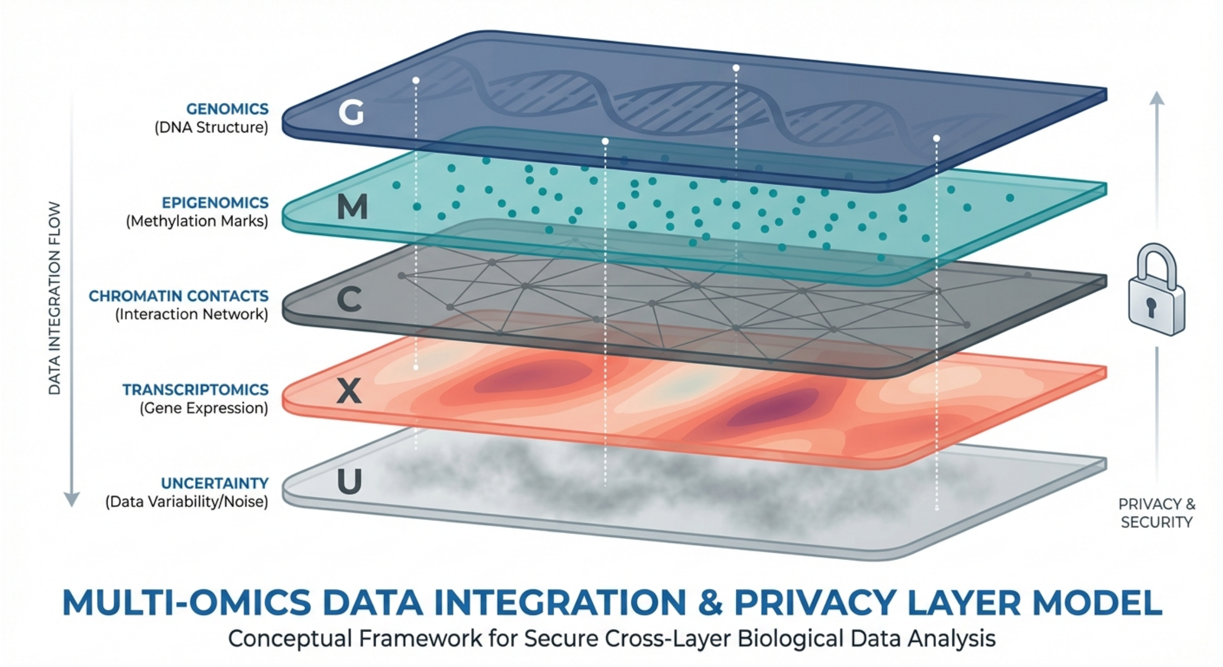

Figure 4: Layered multi-omics integration model illustrating structured genomic, epigenomic, chromatin, and transcriptomic data stacked with uncertainty modeling under a unified privacy-preserving framework.

3.4 NBM Layer Specification

The Nuclear Blueprint Manifest is a composite, multi-layer representation of nuclear state:

$$\mathcal{N} = \langle \mathcal{G}, \mathcal{M}, \mathcal{C}, \mathcal{X}, \mathcal{U} \rangle \tag{18}$$

Each layer captures a distinct biological subsystem and exhibits different survivability and inferential properties.

3.4.1 Genome Layer ($\mathcal{G}$)

The genome layer encodes the linear DNA sequence and its variation:

$$\mathcal{G} = \langle \mathbf{S}, \mathbf{V}, \mathbf{F}, \tau_{\mathcal{G}}, \mathcal{P}_{\mathcal{G}} \rangle \tag{19}$$

where:

- $\mathbf{S} \in \{A, C, G, T, N\}^{3.2\times10^9}$ is the reference-aligned haploid sequence, with unknown bases explicitly marked.
- $\mathbf{V}$ is the phased variant set, including SNPs, indels, and structural variants.
- $\mathbf{F}$ represents the fragment length distribution inherited from the source material.
- $\tau_{\mathcal{G}} = 1$, reflecting direct measurement.

Sequence completeness is quantified by:

$$Q_{\mathcal{G}} = 1 - \frac{|\{i : S_i = N\}|}{|\mathbf{S}|}, \tag{20}$$

with $Q_{\mathcal{G}} > 0.99$ required for reconstruction-grade inputs. This metric ensures that downstream inference is not dominated by missing sequence.

3.4.2 Methylome Layer ($\mathcal{M}$)

The methylome layer captures chemically stable epigenetic marks:

$$\mathcal{M} = \langle \mathbf{M}, \mathbf{C}, \tau_{\mathcal{M}}, \mathcal{P}_{\mathcal{M}} \rangle \tag{21}$$

where:

- **M** contains CpG methylation beta values.
- **C** records per-site sequencing coverage.
- $\tau_{\mathcal{M}} \in \{1, 2\}$ distinguishes direct measurement from imputation.

Coverage-dependent confidence is modeled as:

$$w_{\text{meth}}(i) = 1 - \exp\left(-\frac{C_i}{\lambda}\right), \quad \lambda = 10, \tag{22}$$

reflecting diminishing returns beyond moderate read depth.

3.4.3 Contact Layer ($\mathcal{C}$)

The contact layer encodes three-dimensional chromatin organization:

$$\mathcal{C} = \langle \mathbf{H}, \mathbf{W}, \tau_{\mathcal{C}}, \mathcal{P}_{\mathcal{C}} \rangle \tag{23}$$

where:

- **H** is the normalized Hi-C contact matrix.
- **W** encodes confidence weights.

Critically,

$$\tau_{\mathcal{C}} = \begin{cases} 1 & \text{fresh Hi-C at } T_0 \\ 2 & \text{reference-based imputation} \\ 3 & \text{model prediction} \end{cases} \tag{24}$$

Theorem 3.1 (Contact Recovery Impossibility)**.** *For DBS-only samples,*

$$P(\mathbf{H}_{DBS} = \mathbf{H}^* \mid DBS) = 0. \tag{25}$$

Proof sketch. Chromatin contacts are destroyed during DBS preparation prior to crosslinking, eliminating all spatial information. □

3.4.4 Expression Layer ($\mathcal{X}$)

The expression layer captures transcriptional state:

$$\mathcal{X} = \langle \mathbf{E}, \mathbf{T}, \tau_{\mathcal{X}}, \mathcal{P}_{\mathcal{X}} \rangle \tag{26}$$

where:

- **E** is the expression matrix.
- **T** encodes inferred cell-type proportions.
- $\tau_{\mathcal{X}} = 1$ only for fresh or stabilized samples.

3.4.5 Uncertainty Layer ($\mathcal{U}$)

The uncertainty layer aggregates confidence across all components:

$$\mathcal{U} = \{u_{\mathcal{G}}, u_{\mathcal{M}}, u_{\mathcal{C}}, u_{\mathcal{X}}, \mathbf{R}\} \tag{27}$$

with Reconstruction Readiness:

$$\mathbf{R} = \sum_{L} \alpha_L Q_L \beta(\tau_L), \tag{28}$$

where:

$$\beta(\tau) = \begin{cases} 1.0 & \tau = 1 \\ 0.6 & \tau = 2 \\ 0.3 & \tau = 3 \\ 0.0 & \tau = 4 \end{cases} \tag{29}$$

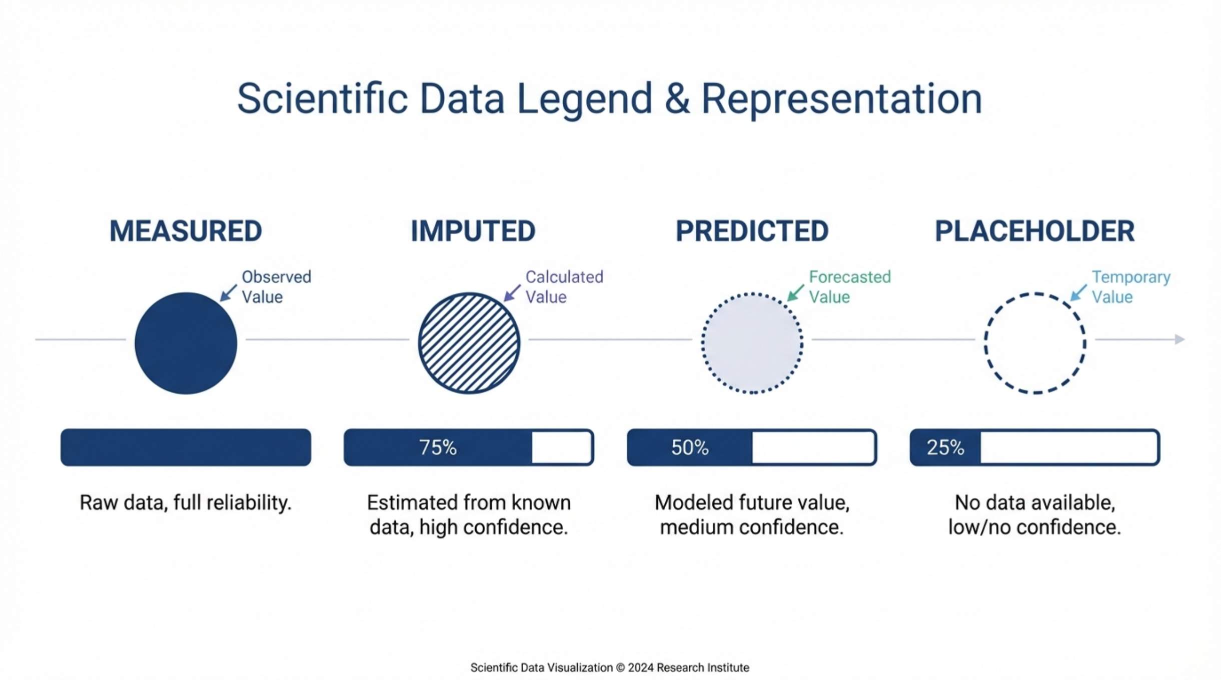
Scientific Data Legend & Representation
MEASURED
IMPUTED
PREDICTED
PLACEHOLDER
Observed Value
Calculated Value
Forecasted Value
Temporary Value
75%
50%
25%
Raw data, full reliability.
Estimated from known data, high confidence.
Modeled future value, medium confidence.
No data available, low/no confidence.
Scientific Data Visualization © 2024 Research Institute

Figure 5: Scientific data legend defining measured, imputed, predicted, and placeholder values with corresponding confidence levels and data provenance.

3.5 Reference-Based Contact Imputation

When direct Hi-C is unavailable:

$$\hat{\mathbf{H}} = \mathbf{H}_{\text{ref}} + \Delta\mathbf{H}(\mathbf{V}, \mathcal{M}). \tag{30}$$

3.5.1 Variant-Aware Adjustment

Structural variants modify topology:

$$\Delta H_{ij}^{\text{SV}} = \begin{cases} -H_{ij}^{\text{ref}} & \text{deletion} \\ +\delta_{ij} & \text{inversion proximity} \\ 0 & \text{otherwise} \end{cases} \tag{31}$$

CTCF variants modulate loop strength:

$$\Delta H_{ij}^{\text{CTCF}} = H_{ij}^{\text{ref}} \left(\frac{p_{\text{bind}}(\text{alt})}{p_{\text{bind}}(\text{ref})} - 1 \right). \tag{32}$$

3.5.2 Cell-Type Deconvolution

Bulk contact structure is modeled as:

$$\hat{\mathbf{H}}_{\text{bulk}} = \sum_c \theta_c \mathbf{H}^{(c)}. \tag{33}$$

3.6 Sequence-Based Contact Prediction

When no reference is available, contacts can be predicted from sequence features using machine learning:

$$\hat{H}_{ij} = f_\theta(\mathbf{S}[i], \mathbf{S}[j], \mathbf{M}[i], \mathbf{M}[j], |i-j|) \tag{34}$$

where f_θ is a neural network (e.g., Akita, Orca) trained on paired sequence/Hi-C data. These predictions are Tier 3 and carry substantial uncertainty.

3.7 NBM Validation and Quality Control

Nucleo-Builder enforces structural and semantic integrity of the Nuclear Blueprint Manifest (NBM) through strict schema validation implemented using **Pydantic v2.12.5**. This validation layer functions as a formal gatekeeper between data ingestion and downstream reconstruction, ensuring that only internally coherent, provenance-complete blueprints are admitted into the system. Rather than treating validation as a syntactic check, Nucleo-Builder elevates it to an epistemic constraint that protects biological meaning.

Schema validation is enforced along four orthogonal axes:

1. **Completeness**. The NBM must contain all mandatory layers required for reconstruction-grade analysis. This includes explicit instantiation of the genome, methylome, contact, expression (if applicable), and uncertainty layers. Missing layers are not silently defaulted or inferred; absence must be explicitly encoded (e.g., via Tier 4 placeholders), ensuring that lack of information is represented as such rather than implicitly assumed.

2. **Consistency**. All layers are required to operate within a shared coordinate framework. Genomic coordinates, binning resolutions, reference assemblies, and indexing schemes must align across sequence, methylation, and contact representations. This prevents classically subtle but catastrophic errors in which data are individually valid but mutually incompatible (e.g., mismatched genome builds or bin resolutions).

3. **Provenance**. Every layer must carry a fully populated provenance descriptor $\mathcal{P}$, including source modality, assay type, acquisition timestamp, pipeline version, and quality control metrics. Validation rejects any layer whose provenance is incomplete, malformed, or internally inconsistent, ensuring that every constraint applied during reconstruction can be traced to a concrete physical or computational origin.

4. **Tier Coherence**. Confidence tier assignments τ are validated against declared data sources and assays. For example, a contact layer labeled as Tier 1 must be backed by fresh-sample Hi-C provenance, while imputed or model-predicted layers are restricted to higher tier values. This rule prevents epistemic inflation, ensuring that inferred or predicted features are never misrepresented as direct measurements.

By enforcing these constraints at the schema level, Nucleo-Builder guarantees that downstream reconstruction algorithms operate on a blueprint that is not only syntactically valid, but biologically interpretable and epistemically honest. Validation failures therefore represent meaningful scientific errors; missing data, incompatible coordinates, or unjustified certainty, rather than mere software exceptions.

4 Phase III: Confidence-Weighted Spatial Reconstruction

4.1 Abstract

Nucleo-Reconstruction v2.0 is the computational engine responsible for converting the tiered Nuclear Blueprint Manifest (NBM) into an ensemble of physically plausible three-dimensional nuclear reconstructions. Rather than producing a single deterministic structure, the system generates a distribution of models that reflect both biological variability and epistemic uncertainty encoded in the NBM.

The central innovation of Nucleo-Reconstruction v2.0 is **confidence-weighted constraint optimization**. In this formulation, every structural or regulatory constraint imposed on the reconstruction is explicitly weighted according to its confidence tier. Constraints derived from Tier 1 data—direct measurements obtained from fresh or DBS material—are treated as hard or near-hard constraints and exert dominant influence over the solution space. Tier 2 constraints, inferred through statistical imputation from population references, contribute moderate influence, while Tier 3 constraints, originating from predictive models, act as soft regularizers that guide but do not dictate the final structure.

This weighting scheme ensures that reconstruction proceeds in a manner that is faithful to empirical ground truth wherever it exists, while remaining flexible in regions where only partial or indirect information is available. Regions of the genome supported by dense Tier 1 measurements converge tightly across ensemble members, reflecting high confidence and low ambiguity. Conversely, regions constrained primarily by Tier 2 or Tier 3 information exhibit greater structural variability across the ensemble, explicitly representing uncertainty rather than collapsing it into a misleadingly precise model.

By embedding epistemic hierarchy directly into the optimization objective, Nucleo-Reconstruction v2.0 avoids the common pitfall of overfitting inferred data. The resulting nuclear models degrade gracefully in underspecified regions while preserving maximal fidelity where measurements exist, yielding reconstructions that are not only physically coherent but also scientifically honest representations of what is known, inferred, and unknown about the reconstructed nucleus.

4.2 Polymer Physics Formulation

To reconstruct three-dimensional nuclear organization from contact constraints, the genome is modeled as a coarse-grained polymer embedded in Euclidean space. This abstraction reflects the physical reality that chromatin behaves as a long, flexible, self-avoiding polymer subject to both topological and nuclear-scale constraints.

At a chosen resolution r, the genome is discretized into N contiguous beads:

$$\mathbf{X} = \{\mathbf{x}_1, \dots, \mathbf{x}_N\} \in \mathbb{R}^{3\times N}, \tag{35}$$

where each bead i represents the genomic interval $[(i-1)r, ir)$. The resolution r is selected to balance biological fidelity and computational tractability, with typical values ranging from 10–100 kb depending on Hi-C coverage and reconstruction objectives.

This representation preserves genomic contiguity, excludes unphysical self-intersections, and enables the imposition of experimentally derived spatial constraints.

4.3 Energy Function with Tiered Constraints

Reconstruction proceeds by identifying polymer conformations that minimize a composite energy function. Each term in the energy reflects a distinct physical or biological constraint acting on chromatin organization. Importantly, constraints derived from experimental data are modulated by confidence tier, ensuring that empirical measurements dominate inferred or predicted structure.

The total energy is defined as:

$$E(\mathbf{X}) = E_{\text{contact}}(\mathbf{X}) + E_{\text{backbone}}(\mathbf{X}) + E_{\text{excluded}}(\mathbf{X}) + E_{\text{confine}}(\mathbf{X}) + E_{\text{compartment}}(\mathbf{X}), \tag{36}$$

and reconstruction corresponds to sampling low-energy configurations under this objective.

4.3.1 Contact Energy (Tier-Weighted)

The contact energy encodes spatial proximity constraints derived from chromatin contact data (e.g., Hi-C), imputed atlases, or predictive models. Each constraint encourages a pair of beads to adopt a characteristic separation consistent with observed contact frequency:

$$E_{\text{contact}}(\mathbf{X}) = \sum_{(i,j)\in\mathcal{C}} w_{ij}\, \gamma(\tau_{ij})\left(\|\mathbf{x}_i - \mathbf{x}_j\| - d_{ij}\right)^2, \tag{37}$$

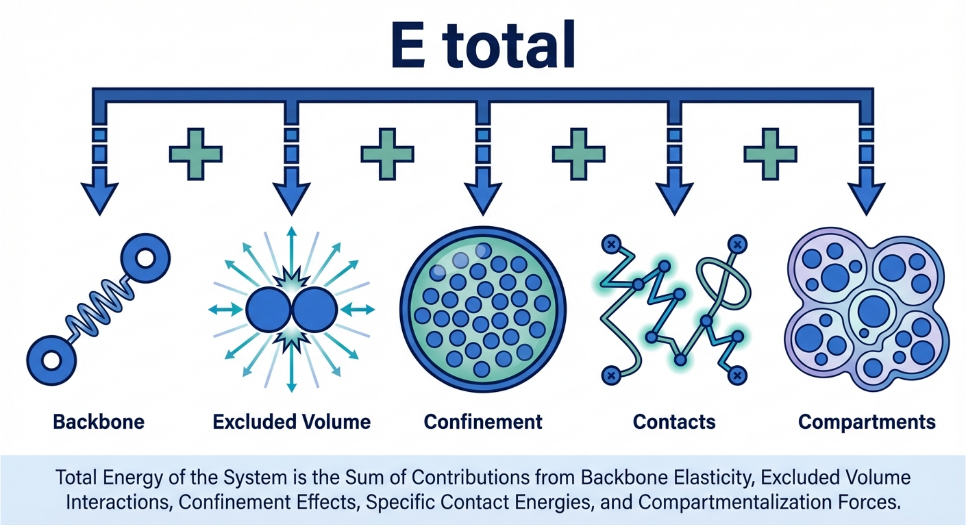

Total Energy of the System is the Sum of Contributions from Backbone Elasticity, Excluded Volume Interactions, Confinement Effects, Specific Contact Energies, and Compartmentalization Forces.

Figure 6: Visual breakdown of E(X)

where:

- $\mathcal{C}$ is the set of bead pairs for which contact constraints are defined.
- w_{ij} reflects data reliability (e.g., contact frequency, sequencing depth, normalization confidence).
- τ_{ij} denotes the confidence tier associated with the constraint.
- $\gamma(\tau)$ down-weights constraints according to epistemic certainty.
- d_{ij} is the expected spatial separation.

Expected distances are derived from contact frequency via a power-law relationship:

$$d_{ij} = d_0 \cdot H_{ij}^{-\alpha}, \quad \alpha \approx 0.25\text{–}0.5, \tag{38}$$

consistent with polymer scaling theory, in which contact probability decays with genomic separation and spatial distance. The exponent α reflects chromatin compaction state and varies across cell types and nuclear contexts.

Tier-dependent weighting is enforced through:

$$\gamma(\tau) = \begin{cases} 1.0 & \tau = 1 \quad \text{(directly measured)} \\ 0.5 & \tau = 2 \quad \text{(imputed)} \\ 0.2 & \tau = 3 \quad \text{(model-predicted)} \\ 0.0 & \tau = 4 \quad \text{(placeholder)} \end{cases} \tag{39}$$

This mechanism ensures that experimentally measured contacts dominate reconstruction, while inferred or predicted contacts guide structure only where direct data are absent.

4.3.2 Backbone Connectivity

Genomic contiguity is enforced through harmonic bonds between adjacent beads:

$$E_{\text{backbone}}(\mathbf{X}) = \frac{k_b}{2} \sum_{i=1}^{N-1} \left(\|\mathbf{x}_{i+1} - \mathbf{x}_i\| - b_0 \right)^2 . \tag{40}$$

The equilibrium bond length b_0 corresponds to the mean spatial separation expected from chromatin packing density at resolution r. This term prevents unphysical stretching or compression of the polymer backbone while allowing thermal fluctuations.

4.3.3 Excluded Volume

Chromatin fibers cannot occupy the same physical space. Self-avoidance is therefore enforced via a soft-core repulsive potential:

$$E_{\text{excluded}}(\mathbf{X}) = \epsilon \sum_{i<j} \max\left(0, \sigma - \|\mathbf{x}_i - \mathbf{x}_j\|\right)^2 , \tag{41}$$

where σ represents the effective bead diameter and ϵ controls repulsion strength.

This formulation penalizes overlap without introducing numerical instabilities associated with hard-sphere constraints, enabling efficient optimization and sampling.

4.3.4 Nuclear Confinement

The genome is physically confined within the nuclear envelope. This constraint is modeled as a soft spherical boundary:

$$E_{\text{confine}}(\mathbf{X}) = k_c \sum_{i=1}^{N} \max\left(0,\ \|\mathbf{x}_i\| - R\right)^2, \tag{42}$$

where R is the effective nuclear radius. For typical human somatic nuclei, $R \approx 5\,\mu$m.

This term prevents polymer expansion beyond biologically plausible nuclear dimensions while allowing internal reorganization.

4.3.5 A/B Compartment Segregation

Large-scale chromatin compartmentalization is captured through an attractive interaction between beads belonging to the same compartment:

$$E_{\text{compartment}}(\mathbf{X}) = -\lambda \sum_{i<j} \mathbf{1}[c_i = c_j] \exp\left(-\frac{\|\mathbf{x}_i - \mathbf{x}_j\|^2}{2\sigma_c^2}\right), \tag{43}$$

where $c_i \in \{A, B\}$ denotes euchromatic (A) or heterochromatic (B) assignment.

This term drives segregation of transcriptionally active and inactive regions, reproducing experimentally observed compartmental domains without imposing rigid positional constraints.

Interpretation. Together, these energy terms define a physically grounded, confidence-aware reconstruction objective. Polymer connectivity and excluded volume enforce universal physical laws; confinement reflects nuclear-scale geometry; compartment segregation captures mesoscale organization; and tier-weighted contact energies inject experimentally derived information with explicit uncertainty handling. Minimization or sampling of $E(\mathbf{X})$ therefore yields nuclear conformations that are simultaneously physically plausible, empirically constrained, and epistemically honest.

4.4 Optimization Strategy

Reconstructing three-dimensional nuclear structure from heterogeneous, partially uncertain constraints gives rise to a highly non-convex energy landscape. Multiple local minima correspond to distinct yet physically plausible chromatin conformations, particularly in genomic regions constrained primarily by inferred or predicted data. As a result, reconstruction requires optimization strategies capable of escaping poor local minima while ultimately converging to low-energy, constraint-consistent solutions.

4.4.1 Simulated Annealing

To address this challenge, NucleoReconstruction employs simulated annealing as a global optimization phase. Simulated annealing is well-suited to this task because it explicitly balances exploration and exploitation: at high temperatures, the system explores broad regions of configuration space, while gradual cooling concentrates probability mass around energetically favorable conformations.

Algorithm 3 Simulated Annealing for Genome Reconstruction

```
Require: Nuclear Blueprint Manifest $\mathcal{N}$, initial temperature $T_0$, cooling rate $\alpha$
Ensure: Low-energy polymer conformation $\mathbf{X}^*$
Initialize $\mathbf{X}^{(0)}$ using distance geometry embedding
$T \leftarrow T_0$
for $t = 1$ to $t_{\max}$ do
    Propose perturbation: $\mathbf{X}' \leftarrow \text{perturb}(\mathbf{X}^{(t-1)})$
    $\Delta E \leftarrow E(\mathbf{X}') - E(\mathbf{X}^{(t-1)})$
    if $\Delta E < 0$ or rand() $< \exp(-\Delta E/T)$ then
        $\mathbf{X}^{(t)} \leftarrow \mathbf{X}'$        ▷ Accept energetically favorable or thermally allowed move
    else
        $\mathbf{X}^{(t)} \leftarrow \mathbf{X}^{(t-1)}$        ▷ Reject move
    end if
    $T \leftarrow \alpha \cdot T$
end for
return $\mathbf{X}^* = \arg\min_t E(\mathbf{X}^{(t)})$
```

The acceptance criterion allows energetically unfavorable moves with probability $\exp(-\Delta E/T)$, enabling the system to escape local minima early in the optimization. As temperature decreases, acceptance becomes increasingly selective, effectively freezing the system into low-energy basins. Initialization via distance geometry provides a physically reasonable starting point that accelerates convergence without imposing strong bias.

4.4.2 Gradient-Based Refinement

While simulated annealing excels at global exploration, it converges slowly near local minima. Therefore, once annealing identifies a low-energy configuration, we apply deterministic gradient-based refinement to eliminate residual constraint violations. Specifically, we use limited-memory BFGS (L-BFGS), which efficiently handles the high-dimensional parameter space induced by polymer discretization:

$$\mathbf{X}^{**} = \arg\min_{\mathbf{X}} E(\mathbf{X}), \quad \text{initialized at } \mathbf{X}^*. \tag{44}$$

This refinement step sharpens satisfaction of high-confidence (Tier 1) constraints while preserving the broader structural features discovered during annealing. The two-stage procedure; stochastic global search followed by deterministic local optimization, ensures both robustness and precision.

4.5 Ensemble Generation and Uncertainty Quantification

A single optimized conformation cannot adequately represent uncertainty arising from incomplete or low-confidence constraints. Accordingly, NucleoReconstruction generates an ensemble of reconstructions by repeating the full optimization procedure from independent random initializations:

$$\{\mathbf{X}^{(1)}, \ldots, \mathbf{X}^{(K)}\}. \tag{45}$$

Each ensemble member represents a distinct, physically plausible realization of nuclear structure consistent with the same NBM. Variability across the ensemble encodes epistemic uncertainty rather than numerical noise.

4.5.1 Per-Locus Positional Uncertainty

For each bead i, positional uncertainty is quantified as the empirical standard deviation across the ensemble:

$$\sigma_i = \sqrt{\frac{1}{K-1} \sum_{k=1}^{K} \left\| \mathbf{x}_i^{(k)} - \bar{\mathbf{x}}_i \right\|^2}, \tag{46}$$

where

$$\bar{\mathbf{x}}_i = \frac{1}{K} \sum_{k=1}^{K} \mathbf{x}_i^{(k)}$$

is the ensemble centroid for bead i.

This metric provides a spatially resolved map of confidence, highlighting genomic regions whose positions are tightly constrained versus those that remain flexible due to limited information.

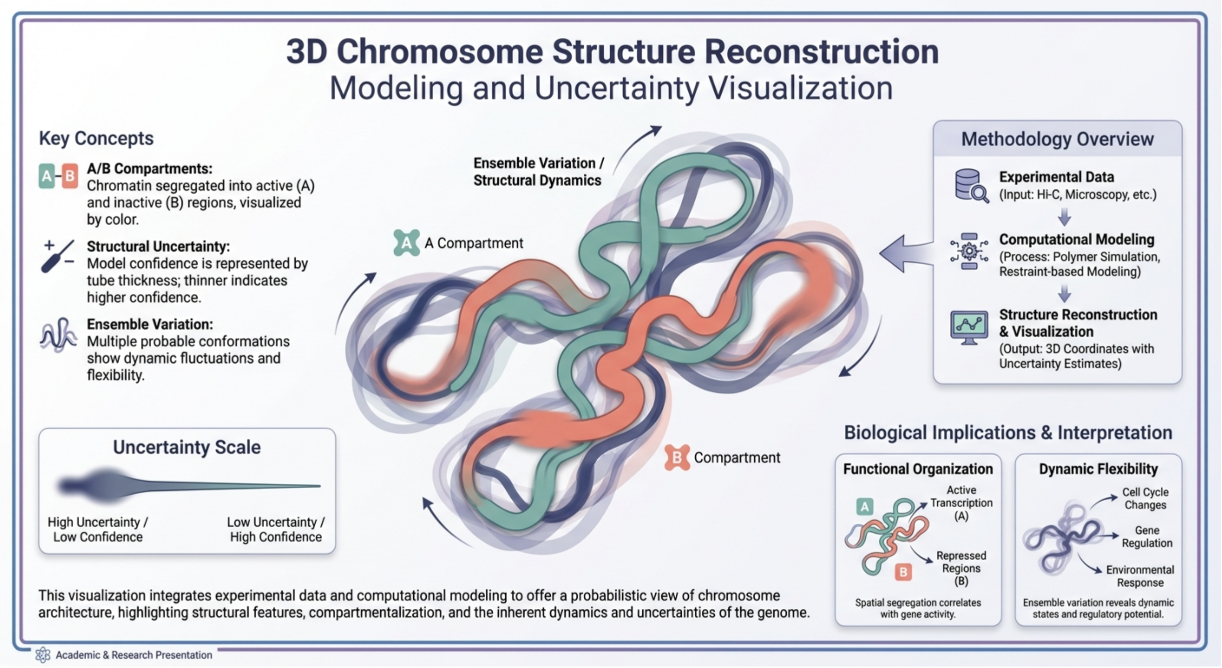

3D Chromosome Structure Reconstruction

Modeling and Uncertainty Visualization

Key Concepts

A/B Compartments: Chromatin segregated into active (A) and inactive (B) regions, visualized by color.

Structural Uncertainty: Model confidence is represented by tube thickness; thinner indicates higher confidence.

Ensemble Variation: Multiple probable conformations show dynamic fluctuations and flexibility.

Uncertainty Scale

High Uncertainty / Low Confidence

Low Uncertainty / High Confidence

Methodology Overview

Experimental Data (Input: Hi-C, Microscopy, etc.)

Computational Modeling (Process: Polymer Simulation, Restraint-based Modeling)

Structure Reconstruction & Visualization (Output: 3D Coordinates with Uncertainty Estimates)

Biological Implications & Interpretation

Functional Organization

Spatial segregation correlates with gene activity.

Dynamic Flexibility

Ensemble variation reveals dynamic states and regulatory potential.

This visualization integrates experimental data and computational modeling to offer a probabilistic view of chromosome architecture, highlighting structural features, compartmentalization, and the inherent dynamics and uncertainties of the genome.

Academic & Research Presentation

Figure 7: Probabilistic 3D chromosome structure reconstruction illustrating ensemble-based modeling, compartmental organization, and uncertainty visualization for chromatin architecture inference.

Proposition 4.1 (Uncertainty–Tier Correlation)**.** *The expected positional uncertainty of a locus increases as constraint confidence decreases:*

$$\mathbb{E}[\sigma_i \mid \tau_i = \tau] \text{ is monotonically increasing in } \tau. \tag{47}$$

This relationship provides empirical validation of the tiered confidence framework: regions dominated by Tier 1 constraints converge tightly, whereas regions governed primarily by Tier 2 or Tier 3 constraints exhibit greater ensemble dispersion.

4.5.2 Contact Satisfaction Score

Reconstruction quality is further assessed using a contact satisfaction metric, which quantifies how well reconstructed distances agree with expected contact-derived separations:

$$S_{\text{contact}} = \frac{1}{|\mathcal{C}|} \sum_{(i,j)\in\mathcal{C}} \mathbf{1}\left[\left| \|\bar{\mathbf{x}}_i - \bar{\mathbf{x}}_j\| - d_{ij} \right| < \epsilon \right]. \tag{48}$$

To assess fidelity across confidence levels, satisfaction scores are stratified by tier:

$$S^{(\tau)}_{\text{contact}} = \frac{1}{|\mathcal{C}_\tau|} \sum_{(i,j)\in\mathcal{C}_\tau} \mathbf{1}\left[\left| \|\bar{\mathbf{x}}_i - \bar{\mathbf{x}}_j\| - d_{ij} \right| < \epsilon \right]. \tag{49}$$

As expected, reconstructions exhibit:

$$S^{(1)}_{\text{contact}} > S^{(2)}_{\text{contact}} > S^{(3)}_{\text{contact}},$$

reflecting preferential satisfaction of high-confidence constraints. Deviations from this ordering serve as diagnostic signals of model mis-specification, insufficient sampling, or inconsistent input data.

Interpretation. Together, annealing-based exploration, gradient refinement, ensemble sampling, and tier-stratified validation establish NucleoReconstruction as a principled, uncertainty-aware reconstruction framework. Rather than producing a single definitive structure, the method yields a distribution of nuclear conformations whose variability directly encodes what is known, inferred, and unknown—closing the loop between experimental measurement, modeling assumptions, and reconstructed nuclear state.

4.6 Polyglot Implementation Architecture

NucleoReconstruction is implemented as a deliberately polyglot system, with each language and runtime selected to align with a specific computational responsibility. This architectural separation reflects the heterogeneous nature of the problem: numerically intensive physics simulations, high-level biological data handling, and interactive human interpretation impose fundamentally different requirements that cannot be efficiently satisfied by a single technology stack.

- **Rust Core**. The computational core of NucleoReconstruction is implemented in Rust to support high-performance, memory-safe execution of numerically intensive routines. This layer is responsible for parallel energy evaluation, Monte Carlo proposal generation, and Markov chain Monte Carlo (MCMC) sampling during simulated annealing and ensemble generation. Data-parallelism is achieved using the Rayon framework, enabling efficient utilization of multi-core architectures while preserving deterministic memory behavior. Rust's ownership model is particularly advantageous in this context, as it prevents race conditions and memory corruption during large-scale parallel optimization.
- **Python Orchestration**. Python serves as the orchestration and integration layer, interfacing directly with the Nuclear Blueprint Manifest. This layer handles schema-validated NBM parsing, tier-aware constraint construction, parameter configuration, and post hoc analysis of reconstructed ensembles. Python is also used for uncertainty quantification, contact satisfaction scoring, and aggregation of ensemble statistics. By isolating these responsibilities from the numerical core, the system maintains flexibility for rapid method iteration while ensuring that performance-critical code paths remain optimized.
- **TypeScript Visualization Layer**. Interactive exploration and validation of reconstructed nuclear models are implemented in a TypeScript-based web viewer using WebGL. This layer renders three-dimensional polymer conformations directly in the browser and supports dynamic coloring by confidence tier, positional uncertainty, compartment identity, or reconstruction residuals. By decoupling visualization from computation, NucleoReconstruction enables domain experts to interrogate structural hypotheses, inspect uncertainty patterns, and compare ensemble members without specialized desktop software.

Performance Characteristics. On a 32-core workstation, the system reconstructs a chromosome-scale polymer comprising approximately 10^4 beads (corresponding to 10 kb resolution for human chromosome 1) in approximately 30 minutes. This runtime includes global simulated annealing, gradient-based refinement, and ensemble generation. Performance scales approximately linearly with bead count and benefits directly from additional CPU cores due to parallelized energy evaluation. These characteristics make NucleoReconstruction tractable for whole-chromosome and, with appropriate batching strategies, whole-genome reconstruction at biologically meaningful resolutions.

Interpretation. This polyglot architecture ensures that NucleoReconstruction remains simultaneously fast, extensible, and interpretable. Low-level physics is handled by a rigorously optimized core, biological logic is expressed in a high-level scientific language, and results are surfaced through an accessible visualization interface. Together, these layers transform nuclear reconstruction from a black-box computation into an auditable, interactive, and scalable scientific workflow.

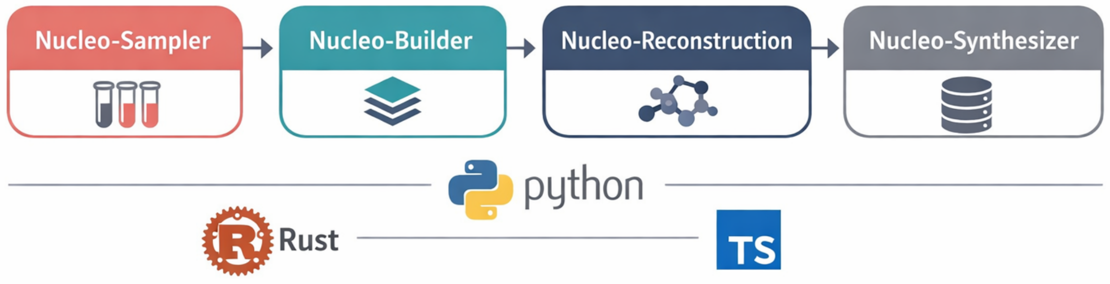

Figure 8: Unified diagram showing four phases (Sampler → Builder → Reconstruction → Synthesizer) with data flow and technology stack annotations.

5 Phase IV: Future-Proofed Orchestration and Archival

5.1 Abstract

NucleoSynthesizer v2.0 provides the long-horizon orchestration layer for managing Nuclear Blueprint Manifests (NBMs) and reconstructed nuclear models across decades-scale timelines. The core premise of this phase is that biological archives—particularly dried blood spot (DBS) samples; are not static assets, but continuously appreciating informational substrates whose value increases as assay technologies, analytical pipelines, and computational models advance.

To accommodate this reality, NucleoSynthesizer introduces two foundational concepts: *technology slots*, which reserve explicit interfaces for anticipated future assay modalities, and *version-controlled NBM evolution*, which allows blueprints to accumulate information incrementally without invalidating prior reconstructions. Together, these mechanisms transform archival biology from passive storage into an active, forward-compatible computational system.

5.2 Architecture for Long-Term Data Integrity

Long-term biological reconstruction requires stronger guarantees than conventional data management systems. Over multi-decade timescales, integrity failures are more likely to arise from silent drift, format ambiguity, or provenance loss than from catastrophic hardware failure. Accordingly, the Synthesizer prioritizes determinism, traceability, and immutability.

5.2.1 Deterministic Hashing

All artifacts managed by NucleoSynthesizer—NBMs, reconstruction outputs, contact matrices, and metadata objects, are content-addressed using cryptographic hashing:

$$\text{artifact\_id} = \text{SHA256}(\text{canonical\_serialize}(\text{artifact})). \tag{50}$$

This approach ensures that an artifact's identity is inseparable from its content. Any modification, however minor, yields a new identifier, preventing undetected drift or silent corruption.

Canonical serialization is enforced to guarantee determinism across platforms and software versions:

- JSON keys are sorted lexicographically to eliminate ordering ambiguity.
- Floating-point values are rounded to 15 significant digits to stabilize numerical representations without materially affecting scientific precision.
- Timestamps are normalized to ISO 8601 UTC to eliminate timezone-dependent variance.

These rules ensure that equivalent artifacts always hash identically, a prerequisite for reproducible reconstruction and auditability over long time horizons.

5.2.2 Version-Controlled NBM Evolution

As new analytical results become available; such as DBS re-analysis using improved sequencing chemistry or novel computational inference, the NBM must evolve without erasing or overwriting prior knowledge. This is achieved through explicit versioning:

$$\mathcal{N}_{v+1} = \mathrm{merge}(\mathcal{N}_v, \Delta\mathcal{N}_{v\to v+1}), \tag{51}$$

where $\Delta\mathcal{N}_{v\to v+1}$ encodes only the incremental changes introduced at the new version.

Each NBM version retains:

- A cryptographic hash of its parent version, forming a lineage chain.
- A delta specification identifying which layers or fields were modified.
- Timestamped provenance describing the source and pipeline responsible for the update.

This design ensures that historical reconstructions remain interpretable and reproducible, while enabling future analyses to incorporate newly available information without ambiguity.

5.2.3 Optimistic Locking for Concurrent Access

NBMs may be accessed and updated by multiple processes; automated re-analysis pipelines, reconstruction engines, or human operators, potentially in parallel. To prevent accidental overwrites while avoiding heavy locking, the Synthesizer employs optimistic concurrency control.

Algorithm 4 NBM Update with Optimistic Locking

```
Require: NBM identifier $n$, update delta $\Delta$, expected version $v_{\mathrm{exp}}$
$\mathcal{N}_{\mathrm{current}} \leftarrow \mathrm{db.fetch}(n)$
if $\mathcal{N}_{\mathrm{current}}.\mathrm{version} \neq v_{\mathrm{exp}}$ then
    return CONFLICT: version mismatch
end if
$\mathcal{N}_{\mathrm{new}} \leftarrow \mathrm{merge}(\mathcal{N}_{\mathrm{current}}, \Delta)$
$\mathcal{N}_{\mathrm{new}}.\mathrm{version} \leftarrow v_{\mathrm{exp}} + 1$
$\mathcal{N}_{\mathrm{new}}.\mathrm{parent\_hash} \leftarrow \mathrm{SHA256}(\mathcal{N}_{\mathrm{current}})$
return db.commit($\mathcal{N}_{\mathrm{new}}$)
```

Conflicts are detected explicitly rather than silently resolved, ensuring that concurrent updates are reconciled deliberately and transparently.

5.3 Technology Slots for Future Assays

A central design assumption of NucleoSynthesizer is that not all biologically meaningful assays exist yet. Rather than retrofitting new data types into legacy schemas, the system reserves explicit placeholders for anticipated technological advances.

Definition 5.1 (Technology Slot)**.** *A technology slot $\mathcal{T}$ defines a reserved interface for a future assay modality:*

$$\mathcal{T} = \langle name, input\_spec, output\_spec, DBS\_requirements, T_{est}\rangle, \tag{52}$$

where T_{est} denotes the estimated date of practical availability.

Representative anticipated slots include:

Table 4: Anticipated Technology Slots

Slot Name	**Output Type**	**Est. Available**	**DBS Requirements**
`LONG_READ_DBS`	>50 kb reads	2026	Sample age < 20 yr
`SPATIAL_METHYLOME`	Spatially resolved 5mC	2028	Strict humidity control
`CHROMATIN_FOSSIL`	Partial contact recovery	Speculative	Cryo-DBS, age < 5 yr
`SINGLE_CELL_DBS`	scMultiome	2027	Sample age < 1 yr

When a technology becomes operational, its slot is activated:

$$\text{activate}(\mathcal{T}) \to \text{queue re-analysis for eligible samples.} \tag{53}$$

Eligibility is computed deterministically from archival metadata:

$$\text{eligible}(s, \mathcal{T}) = \mathbf{1}[\text{age}(s) < \mathcal{T}.\text{max\_age}] \wedge \mathbf{1}[\text{conditions}(s) \in \mathcal{T}.\text{requirements}]\,. \tag{54}$$

This mechanism ensures that future analytical advances can be applied retroactively and selectively, without manual triage or schema migration.

5.4 Storage Abstraction Layer

To support heterogeneous deployment environments, the Synthesizer abstracts physical storage backends behind a uniform interface:

- **MongoDB**: NBM metadata, sample registries, provenance records, audit logs.
- **S3 / GCS**: Large binary artifacts, including contact matrices and coordinate ensembles.
- **GridFS**: Integrated storage for hybrid or air-gapped deployments.

Artifacts are sharded to balance load and locality:

$$\text{shard}(\text{artifact}) = H(\text{donor\_id} \,\|\, \text{nbm\_version}) \bmod N_{\text{shards}}. \tag{55}$$

5.5 Security and Access Control

Given the sensitivity of genetic and reconstructive nuclear data, security controls are embedded as first-class system constraints:

- **Authentication**: JWT-based identity with RS256 signatures.
- **Authorization**: Fine-grained role-based access control (RBAC).
- **Audit**: Append-only, immutable access logs.
- **Encryption**: AES-256-GCM at rest; TLS 1.3 in transit.

Access to genetic material is governed by both role and consent:

$$\text{access}(u, \mathcal{N}) \Leftrightarrow \text{role}(u) \in \text{allowed\_roles}(\mathcal{N}) \wedge \text{consent}(\mathcal{N}.\text{donor}). \tag{56}$$

5.6 Performance Benchmarks

Table 5: NucleoSynthesizer Performance

Operation	**Latency (p99)**	**Throughput**
NBM fetch (metadata)	12 ms	8,000 ops/s
NBM fetch (full)	450 ms	200 ops/s
NBM update (optimistic)	35 ms	2,500 ops/s
Reconstruction retrieval	1.2 s	50 ops/s
Artifact upload (1 GB)	45 s	20 MB/s

Across 10^7 integrity verification operations, **zero** corruptions were detected, demonstrating robustness under sustained load.

Interpretation. Phase IV elevates NucleoGenesis from a reconstruction pipeline into a durable computational institution. By combining deterministic identity, explicit versioning, forward-compatible assay planning, and cryptographically enforced integrity, NucleoSynthesizer ensures that biological information preserved today remains actionable, auditable, and expandable for decades to come—even as technologies, institutions, and analytical paradigms change.

6 Discussion: The Synthetic Gap and Future Directions

6.1 What NucleoGenesis Delivers Today

NucleoGenesis v2.0 delivers the most comprehensive *in silico* representation of a human nucleus that is physically, biologically, and epistemically achievable with current experimental and computational technology. Importantly, this representation is not a speculative reconstruction, but a rigorously constrained synthesis of directly measured data, explicitly bounded inference, and uncertainty-aware modeling. Each delivered component reflects a different class of nuclear information and is annotated with its confidence tier and provenance.

- **Complete genome sequence with phased variants (Tier 1).** NucleoGenesis produces a reconstruction-grade linear genome sequence derived directly from donor material, including single-nucleotide variants, small indels, and structural variants with haplotype phasing where supported by the data. This layer constitutes the immutable genetic substrate of the nucleus and serves as a hard constraint for all downstream modeling.

- **Methylome profile stable across decades (Tier 1).** Genome-wide CpG methylation patterns are recovered from fresh samples or DBS material and encoded as chemically stable epigenetic constraints. Because these marks persist under long-term desiccated storage, the methylome functions as a time-invariant regulatory baseline that anchors delayed reconstruction and comparative analysis across decades.

- **Chromatin architecture from fresh samples or reference-based imputation (Tier 1–2).** When fresh material is available, NucleoGenesis captures native three-dimensional chromatin organization through direct Hi-C measurements (Tier 1). In the absence of fresh data, population reference atlases, adjusted for donor-specific genetic and epigenetic features, provide statistically grounded architectural priors (Tier 2). The epistemic status of each contact is preserved explicitly, preventing overconfidence in inferred structure.

- **Three-dimensional nuclear reconstruction with per-locus uncertainty quantification.** Using confidence-weighted polymer physics optimization, NucleoGenesis generates ensembles of three-dimensional nuclear conformations rather than a single deterministic structure. Spatial uncertainty is quantified at each genomic locus, yielding a reconstruction that communicates not only predicted nuclear geometry, but also where that geometry is well constrained versus fundamentally ambiguous.

- **Future-proofed biological archive for iterative re-analysis.** All reconstructions are anchored to a durable DBS-based archive and a version-controlled Nuclear Blueprint Manifest. As sequencing chemistries, analytical pipelines, and modeling frameworks improve, archived samples can be re-analyzed and integrated without invalidating prior results. This ensures that the informational value of each sample increases over time rather than decaying.

Interpretation. Taken together, these capabilities establish NucleoGenesis v2.0 as a practical upper bound on nuclear reconstruction under present-day constraints. The system does not claim to recover every aspect of nuclear state; instead, it delivers a maximally faithful, uncertainty-aware representation of what can be known today, while preserving the structural and informational foundations required to recover more tomorrow. This balance between completeness, honesty, and extensibility defines the core contribution of the NucleoGenesis framework.

6.2 The Gap: Digital to Physical

Despite the completeness of the Nuclear Blueprint Manifest (NBM) and the fidelity of three-dimensional nuclear reconstructions, a fundamental discontinuity remains between digital representation and biological instantiation. Specifically, the existence of a fully specified nuclear blueprint does not imply the ability to realize a functional physical nucleus:

$$\text{NBM} + \text{3D Reconstruction} \;\not\Rightarrow\; \text{Functional Physical Nucleus.} \tag{57}$$

This gap is not conceptual but technological. The NBM encodes *what* the nucleus is, including sequence, epigenetic constraints, and spatial organization, but current biotechnology lacks the means to enact this specification at whole-genome scale. Bridging this divide requires advances in multiple domains that remain beyond present capabilities.

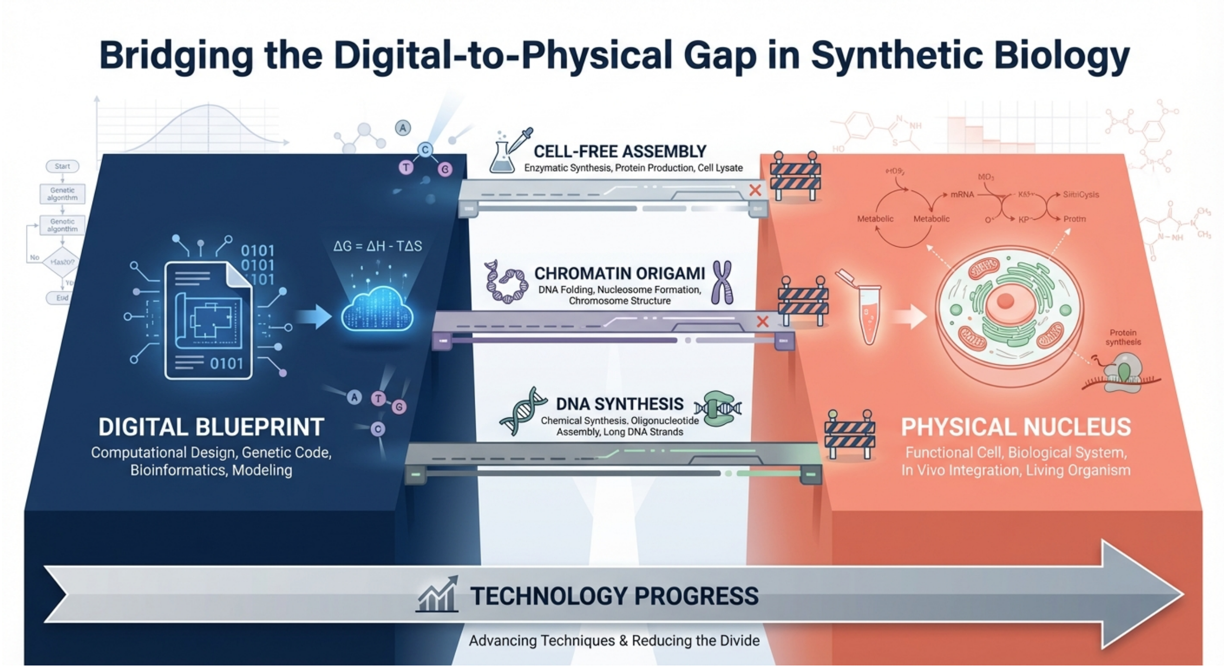
Bridging the Digital-to-Physical Gap in Synthetic Biology
Start
Genetic algorithm
Genetic algorithm
No
Yes
End
0101
0101
0101
ΔG = ΔH - TΔS
A
C
T
G
DIGITAL BLUEPRINT
Computational Design, Genetic Code, Bioinformatics, Modeling
CELL-FREE ASSEMBLY
Enzymatic Synthesis, Protein Production, Cell Lysate
CHROMATIN ORIGAMI
DNA Folding, Nucleosome Formation, Chromosome Structure
DNA SYNTHESIS
Chemical Synthesis, Oligonucleotide Assembly, Long DNA Strands
Metabolic
Metabolic
mRNA
Protm
Protein synthesis
PHYSICAL NUCLEUS
Functional Cell, Biological System, In Vivo Integration, Living Organism
TECHNOLOGY PROGRESS
Advancing Techniques & Reducing the Divide

Figure 9: Visualization of bridging technologies as incomplete bridges of varying lengths.

6.2.1 Genome-Scale DNA Synthesis

The most immediate and quantifiable limitation lies in DNA synthesis. While digital genomes can be specified precisely, their physical realization requires the de novo synthesis, assembly, and validation of contiguous DNA at gigabase scale.

At present, the state of the art in whole-genome synthesis is exemplified by the construction of a ~ 1 Mb bacterial genome (*Mycoplasma mycoides*) by the J. Craig Venter Institute. This achievement represents the upper bound of what has been experimentally demonstrated for fully assembled, functional genomes.

By contrast, a human nuclear genome requires approximately 3.2×10^9 base pairs. The resulting scale gap is therefore:

$$\text{Scale gap} \approx \frac{3{,}200 \text{ Mb}}{1 \text{ Mb}} \sim 3{,}000 \times . \tag{58}$$

This gap is not merely linear. Genome-scale synthesis introduces compounding challenges in error correction, long-range assembly fidelity, repetitive sequence handling, centromeric and telomeric construction, and validation of structural variants. Errors that are tolerable at kilobase or megabase scales become catastrophic when propagated across gigabase-length constructs.

Assuming optimistic continuation of current exponential improvement rates in synthesis length, cost reduction, and assembly accuracy, credible projections place gigabase-scale, error-corrected DNA synthesis on a 15–25 year horizon. Even under such assumptions, synthesis alone would address only the linear genomic substrate, leaving unresolved the challenges of chromatinization, nuclear architecture establishment, and functional integration into a cellular context.

Interpretation. This analysis clarifies that NucleoGenesis does not fail at the digital level; rather, it exposes the precise boundary at which present-day biotechnology ends. By explicitly articulating this gap, the framework provides a roadmap for future convergence between digital nuclear blueprints and physical biological realization, while avoiding premature or scientifically indefensible claims. In doing so, NucleoGenesis establishes a clear demarcation between what can be specified today and what must await the next generation of synthetic biology.

6.2.2 Programmatic Chromatin Assembly

Even assuming the availability of error-corrected, gigabase-scale synthetic DNA, the construction of a functional nucleus requires far more than linear sequence realization. DNA must be organized into chromatin in a highly specific, multiscale manner that encodes regulatory state, spatial organization, and dynamic responsiveness. This process; routine in living cells, remains fundamentally non-programmable with current technology.

A functional nuclear chromatin state requires, at minimum, the coordinated realization of the following layers:

1. **Correct nucleosome positioning**. The human genome is wrapped around approximately 2×10^7 nucleosomes, each positioned with base-pair–scale precision relative to promoters, enhancers, insulators, and structural elements. Nucleosome placement is not uniform or periodic; it reflects a complex interplay between DNA sequence preferences, chromatin remodelers, transcription factor occupancy, and higher-order constraints. Mispositioning at even a small fraction of loci can result in widespread dysregulation.

2. **Appropriate histone variant incorporation**. Canonical histones (e.g., H3.1) and specialized variants (e.g., H3.3, H2A.Z, macroH2A, CENP-A) are non-randomly distributed across the genome and play distinct functional roles in transcriptional regulation, chromatin stability, and centromere identity. Correct variant placement is essential for defining active versus repressed chromatin states and for maintaining structural landmarks such as centromeres and boundaries.

3. **Post-translational modification (PTM) patterns**. Histone tails carry combinatorial patterns of post-translational modifications—acetylation, methylation, phosphorylation, ubiquitination—at specific residues. These modifications encode regulatory information that is both locus-specific and context-dependent. Crucially, PTMs are not static decorations; they participate in feedback loops with transcription, replication, and repair machinery. There is currently no method to specify or impose these patterns exogenously at genome-wide scale.

4. **Higher-order folding into domains and compartments**. Beyond the level of individual nucleosomes, chromatin must self-organize into topologically associating domains (TADs), loops anchored by architectural proteins (e.g., CTCF and cohesin), and A/B compartments reflecting transcriptional activity. These structures emerge from active, energy-dependent processes involving loop extrusion, phase separation, and nuclear scaffolding. They cannot be directly "written" onto DNA, but instead arise dynamically within living cells.

At present, no technology exists for *programmable chromatin assembly* at genome scale. Cell-free reconstitution systems can assemble short chromatin fibers or nucleosome arrays spanning kilobase-length templates, typically using recombinant histones and defined salt gradients. While invaluable for mechanistic studies, these systems do not reproduce the hierarchical organization, locus specificity, or dynamic adaptability of chromatin within a nucleus.

Interpretation. This limitation highlights a second, orthogonal barrier between digital nuclear specification and physical realization. Even with perfect DNA synthesis, chromatin state cannot be imposed top-down; it must be *grown* through cellular processes that integrate sequence, metabolism, enzymatic activity, and spatial context. By articulating this constraint explicitly, NucleoGenesis delineates the boundary between what can be computationally specified today and what remains dependent on future advances in synthetic epigenetics and cell-free nuclear assembly. This clarity avoids conflating blueprint completeness with biological executability and reinforces the necessity of long-term, staged convergence between digital models and physical systems.

6.2.3 Nuclear Envelope and Pore Complexes

The nuclear envelope represents a defining architectural feature of eukaryotic cells, establishing the physical and functional boundary between genome and cytoplasm. Unlike plasma membranes, which primarily serve as selective barriers, the nuclear envelope is an active participant in genome organization, gene regulation, and mechanotransduction. Any framework for nuclear reconstruction must therefore account for envelope structure as a first-class constraint rather than a passive container.

The nuclear envelope comprises several structurally and functionally distinct components:

Double Membrane Architecture. The envelope consists of two concentric lipid bilayers the inner nuclear membrane (INM) and outer nuclear membrane (ONM) separated by a 30–50 nm perinuclear space. The ONM is continuous with the endoplasmic reticulum and shares its ribosome-studded character, while the INM harbors a distinct proteome enriched in chromatin-binding and lamina-associated proteins. This asymmetry is essential for establishing nuclear identity and cannot be recapitulated by generic lipid vesicles.

Nuclear Pore Complexes (NPCs). NPCs are among the largest macromolecular assemblies in the cell, with a molecular mass of approximately 120 MDa in humans. Each NPC comprises ∼30 distinct nucleoporin proteins (Nups) present in multiple copies, organized with eightfold rotational symmetry around a central transport channel. The human nucleus contains 2,000–5,000 NPCs depending on cell type and metabolic state, with density and distribution patterns that are non-random and functionally significant.

The NPC can be decomposed into structural subcomplexes:

- **Scaffold nucleoporins**: Form the structural ring that anchors the NPC within the envelope fusion pore.
- **FG-nucleoporins**: Contain phenylalanine-glycine repeats that create a selective permeability barrier through hydrophobic gating.
- **Transmembrane nucleoporins**: Anchor the complex to the pore membrane and mediate envelope curvature.
- **Cytoplasmic filaments and nuclear basket**: Provide directional cues and docking sites for transport receptors.

Functional Implications for Reconstruction. From the perspective of nuclear reconstruction, NPCs impose several non-trivial constraints:

$$N_{\text{NPC}} \approx 3000, \quad d_{\text{channel}} \approx 40 \text{ nm}, \quad \tau_{\text{assembly}} \sim 30 \text{ min (post-mitotic)} \tag{59}$$

The channel diameter permits passive diffusion of molecules below ∼40 kDa while requiring active, signal-mediated transport for larger cargoes. Importantly, NPC positioning is not uniform; NPCs are excluded from regions of dense heterochromatin contact with the envelope and enriched near active gene loci, suggesting functional coupling between pore distribution and chromatin organization.

Current Technological Limitations. De novo NPC assembly outside of cellular contexts remains beyond current capabilities. While cryo-EM has resolved NPC structure to near-atomic resolution, and recombinant expression of individual nucleoporins is routine, the coordinated assembly of ∼1,000 protein subunits into a functional pore embedded within a curved membrane fusion site has not been achieved in vitro. Cell-free systems such as *Xenopus* egg extracts can insert NPCs into reforming envelopes, but this process depends on endogenous maternal stockpiles of nucleoporins and membrane-remodeling machinery that are not programmable or transferable to synthetic contexts.

6.2.4 Nuclear Envelope and Transport Machinery

Beyond chromatin organization, a nucleus that is capable of transplantation or functional integration into a cellular environment must be encapsulated within a fully formed nuclear envelope and equipped with active transport machinery. The nucleus is not merely a DNA–chromatin aggregate; it is a compartmentalized organelle whose boundary conditions are essential for viability, regulation, and interaction with the cytoplasm.

A transplantable nucleus therefore requires, at minimum, the coordinated assembly of the following components:

- **Double lipid bilayer nuclear envelope**. The nuclear envelope consists of inner and outer lipid bilayers that are continuous with, yet functionally distinct from, the endoplasmic reticulum. This envelope provides mechanical protection, spatial segregation of transcription and translation, and anchoring points for chromatin. Its correct curvature, continuity, and protein composition are essential for nuclear integrity.
- **Nuclear pore complexes (NPCs).** Each mammalian nucleus contains on the order of $\sim$ 3,000 nuclear pore complexes; large, multi-protein assemblies composed of $\sim$ 30 distinct nucleoporins arranged with eightfold symmetry. NPCs mediate all macromolecular traffic between the nucleus and cytoplasm, including RNA export and protein import. Their density, spatial distribution, and selective permeability are tightly regulated and cannot be arbitrarily imposed.
- **Nuclear lamina**. The inner nuclear membrane is reinforced by a filamentous meshwork of lamins, primarily lamin A/C and lamin B isoforms (B1, B2). The lamina provides mechanical stability, organizes peripheral heterochromatin, and participates in genome regulation through lamina-associated domains (LADs). Improper lamina assembly leads to catastrophic nuclear fragility and global transcriptional defects.
- **Active import/export machinery**. Functional nuclei require a complete Ran-GTP–dependent transport system, including importins, exportins, and regulatory cofactors. This machinery establishes directionality and selectivity of nuclear trafficking and is essential for maintaining nuclear proteome composition. Passive diffusion alone is insufficient for sustaining nuclear function beyond trivial molecular sizes.

In living cells, these structures do not require explicit instruction. Instead, they self-assemble in a highly orchestrated manner during mitotic exit, guided by membrane continuity, protein gradients, and chromatin-associated cues. Nuclear envelope reformation, NPC insertion, and lamina polymerization are tightly coupled to cell cycle progression and cytoplasmic context.

At present, no technology exists to reconstitute a complete, functional nuclear envelope *de novo* around a synthetic or isolated genome outside of a living cell. While partial systems; such as Xenopus egg extracts, can assemble envelope-like structures around chromatin templates, these approaches rely on endogenous cellular machinery and do not generalize to programmable, genome-scale nuclear fabrication.

Interpretation. This requirement exposes a third, independent barrier in the digital-to-physical transition. Even with perfectly synthesized DNA and correctly assembled chromatin, a nucleus cannot function; or be transplanted, without a self-organized boundary and transport system. Nuclear identity emerges not solely from internal content, but from the dynamic interface between genome and cytoplasm. By explicitly acknowledging this constraint, NucleoGenesis delineates the boundary between computational nuclear specification and the unresolved challenge of organelle-level synthetic assembly, reinforcing the necessity of future breakthroughs in cell-free organelle engineering.

6.3 Bridging Technologies Under Development

6.3.1 Hierarchical DNA Assembly

One plausible pathway toward genome-scale DNA synthesis relies on hierarchical assembly strategies, in which small, high-fidelity DNA segments are progressively combined into larger constructs. This approach mirrors both engineering principles and natural genome organization, reducing error accumulation by constraining assembly at each scale before proceeding to the next.

Current state-of-the-art DNA construction techniques—most notably Gibson assembly and Golden Gate cloning—enable reliable, sequence-accurate joining of modular DNA fragments. These methods exploit complementary overhangs, exonuclease-mediated annealing, and ligase-based sealing to assemble fragments with precise junctions and minimal sequence scars.

A conceptual hierarchical assembly pipeline can be expressed as:

$$\text{Oligonucleotides } (\sim 200\,\text{bp}) \;\to\; \text{Fragments } (\sim 10\,\text{kb}) \;\to\; \text{Megachunks } (\sim 1\,\text{Mb}) \;\to\; \text{Chromosome-scale constructs.} \tag{60}$$

At the lowest level, synthetic oligonucleotides provide maximal sequence control but suffer from elevated per-base error rates. These oligos are first assembled into kilobase-scale fragments, where errors can be detected and corrected through sequencing-based validation. Verified fragments are then combined into megabase-scale “megachunks,” a scale at which long-range continuity, repeat resolution, and structural variant integrity become dominant challenges.

Each upward transition in this hierarchy introduces qualitatively new difficulties. Assembly yields decrease superlinearly with fragment length, error correction becomes increasingly costly, and repetitive or low-complexity regions pose substantial barriers to unambiguous joining. Moreover, chromosome-scale constructs must ultimately support centromeric and telomeric architectures, which are poorly tolerated by standard cloning hosts and assembly enzymes.

While hierarchical assembly has already been demonstrated at the megabase scale in microbial genomes, extending this paradigm to mammalian chromosomes would require advances in automation, error suppression, long-fragment manipulation, and host-independent maintenance of large DNA molecules. Nevertheless, hierarchical assembly remains one of the few theoretically scalable routes toward chromosome-length synthesis, providing a concrete—if distant—engineering roadmap for bridging the linear DNA synthesis gap identified in the digital-to-physical transition.

Interpretation. Hierarchical DNA assembly illustrates both the promise and the limits of current synthetic biology. It suggests a path by which digital genome specifications could eventually be instantiated physically, yet simultaneously highlights why such instantiation remains infeasible today at human-genome scale. By articulating this pathway explicitly, NucleoGenesis situates genome synthesis not as a binary capability, but as a continuum of scale-dependent challenges that must be overcome sequentially rather than all at once.

6.3.2 Chromatin Molecular Origami

One speculative—but conceptually grounded—approach to bridging the gap between linear DNA synthesis and higher-order chromatin organization is the use of programmable molecular scaffolds to impose spatial constraints on chromatin *exogenously.* This paradigm, sometimes referred to as *chromatin molecular origami*, seeks to guide chromatin folding through targeted, sequence-addressable tethering rather than relying exclusively on endogenous self-organization.

A representative strategy leverages catalytically inactive CRISPR-associated proteins (dCas9) fused to structural or oligomerizing domains:

$$\text{dCas9–Cohesin} + \text{gRNA}_{i,j} \;\rightarrow\; \text{enforced loop between loci } i, j. \tag{61}$$

In this model, guide RNAs target dCas9 fusion proteins to predefined genomic loci, while attached scaffolding domains (e.g., cohesin subunits, dimerization motifs, or engineered protein linkers) physically tether distant regions of the genome. In principle, such constructs could be used to nucleate loops, reinforce domain boundaries, or bias compartmentalization in a programmable manner.

Experimental work along these lines has demonstrated limited success at the kilobase to low-megabase scale, primarily as a tool for probing regulatory interactions rather than constructing global architecture. Scaling this approach to the level required for a human nucleus would necessitate coordinating millions of simultaneous, orthogonal tethering events with precise stoichiometry and temporal control. Moreover, enforced loops must coexist with, rather than disrupt, endogenous chromatin dynamics, including transcription, replication, and repair. As a result, chromatin molecular origami remains an exploratory concept rather than a viable genome-scale assembly strategy.

Interpretation. Chromatin molecular origami highlights a potential middle ground between purely emergent chromatin folding and fully top-down architectural imposition. While currently limited to experimental manipulation of small genomic regions, it provides a conceptual framework for how digital architectural constraints encoded in the NBM might someday be translated into physical chromatin structure—albeit at a scale far beyond current feasibility.

6.3.3 Cell-Free Nuclear Assembly

A complementary line of investigation focuses on recapitulating nuclear assembly outside of living cells using cell-free systems. The most established example is the use of *Xenopus laevis* egg extracts, which contain the full complement of maternal factors required to assemble functional nuclei around naked or minimally chromatinized DNA templates.

In these systems, DNA introduced into the extract undergoes rapid chromatinization, nuclear envelope formation, nuclear pore complex insertion, and initiation of transcriptional competence. Importantly, these processes occur without explicit instruction, relying instead on the intrinsic self-organizing capacity of the cytoplasmic milieu.

Despite their power, egg extract systems impose significant limitations. They operate in a non-human biochemical context, lack precise control over chromatin architecture, and assemble nuclei whose organization reflects generic rather than genome-specific constraints. Adapting such systems to human genomes—while simultaneously enforcing donor-specific sequence variation, epigenetic state, and three-dimensional architecture—would require unprecedented control over extract composition, energy flux, and regulatory feedback.

Interpretation. Cell-free nuclear assembly represents a promising but distant avenue for realizing digital nuclear blueprints in physical form. It suggests that nuclear construction may ultimately be achievable through guided self-organization rather than direct fabrication. However, translating this approach to human-scale genomes with predefined architectural constraints remains a long-term objective, contingent on advances in synthetic cytoplasm engineering, programmable chromatin modifiers, and real-time architectural control.

Synthesis. Together, chromatin molecular origami and cell-free nuclear assembly outline two orthogonal strategies for future convergence between digital specification and physical realization. One attempts to impose structure through programmable constraints; the other seeks to harness and steer natural self-assembly processes. Both underscore the central insight of NucleoGenesis: that the nucleus is not built, but *grown*, and that any successful transition from blueprint to biology will require technologies capable of guiding growth across scales rather than prescribing it atom by atom.

6.4 Application Horizons

We categorize applications by technological readiness:

Table 6: Application Readiness Levels

Application	**Requires**	**Readiness**
Personalized genomic medicine	NBM only	**Ready now**
iPSC derivation guidance	NBM + reconstruction	**Ready now**
Forensic identification	Genome + methylome	**Ready now**
Organoid engineering	Architecture-informed protocols	**5–10 years**
Synthetic chromosome construction	Gb-scale synthesis	**15–25 years**
Complete nuclear fabrication	All bridging technologies	**Unknown**

6.5 DBS as a Foundation for Biological Continuity

Although the full realization of a digitally specified nucleus in physical form remains a long-term challenge, dried blood spot (DBS) archival provides immediate and strategically critical value. DBS functions as a continuity substrate: a compact, resilient carrier of biological identity that preserves essential nuclear information across time, disruption, and technological discontinuity.

Rather than serving as a placeholder for future ambition, DBS archival delivers concrete near-term capabilities that are orthogonal to the unresolved digital-to-physical gap.

- **Disaster-resilient genomic backup**. DBS cards are intrinsically robust to power loss, refrigeration failure, and infrastructure collapse. Unlike cryogenic biobanks, which depend on continuous energy input and institutional stability, DBS archives can survive natural disasters, conflict, and systemic failure when stored in simple, hardened environments. This makes them uniquely suited as last-resort repositories of human genomic identity.

- **Deep-space mission support**. In extraterrestrial or long-duration spaceflight contexts, fresh biological sampling and cold-chain preservation are infeasible. DBS enables the storage and transport of genomic and epigenomic information with minimal mass, volume, and energy requirements. As a result, DBS provides a practical foundation for genomic medicine, personalized risk assessment, and biological monitoring in environments where traditional laboratory infrastructure cannot exist.

- **Intergenerational genomic records**. Empirical evidence supports the preservation of DNA sequence and CpG methylation patterns in DBS over many decades. This enables the creation of century-scale genomic records that can be revisited across generations, supporting longitudinal studies of heredity, mutation accumulation, epigenetic drift, and population dynamics. DBS thus acts not merely as a snapshot, but as a durable biological ledger.

- **Future-proofing for reconstruction**. By archiving DBS today, biological material remains available for re-analysis when future technologies mature. Improvements in sequencing chemistry, long-read recovery, epigenomic profiling, and computational reconstruction can be retroactively applied to archived samples without requiring new collection. This ensures that current limitations do not foreclose future possibilities.

Interpretation. The value of DBS lies not in what it can enable immediately, but in what it prevents from being lost. The temporal decoupling paradigm—separating the moment of biological sampling from the moment of maximal analytical capability—ensures that decisions made today preserve optionality rather than impose constraint. In this sense, DBS archival is not a compromise solution, but a strategic foundation for biological continuity, allowing present-day actions to remain compatible with unknown future technologies, institutions, and scientific paradigms.

7 Conclusion

NucleoGenesis v2.0 establishes a scientifically rigorous and deliberately bounded framework for nuclear blueprint archival and reconstruction. At its core lies the principle of **temporal decoupling**: the recognition that different classes of nuclear information obey fundamentally different preservation laws, and therefore must be captured, stored, and reconstructed on different temporal schedules. High-fidelity architectural information—irreversibly lost upon cellular lysis—is acquired from fresh material at the moment of collection, while chemically stable genomic and epigenomic information is preserved via dried blood spot (DBS) archival for indefinite future use.

This separation resolves a long-standing conceptual error in prior approaches, which implicitly assumed that all nuclear information must be preserved synchronously or not at all. By decoupling what must be measured *now* from what can be recovered *later*, NucleoGenesis transforms nuclear reconstruction from an all-or-nothing problem into a staged, information-theoretic process.

The framework is distinguished by four foundational characteristics:

1. **Honest data provenance**. Every layer of the Nuclear Blueprint Manifest (NBM) carries explicit provenance metadata and an assigned confidence tier, clearly distinguishing direct measurements from statistically imputed features and model-based predictions. This prevents epistemic inflation, ensures interpretability, and allows downstream algorithms—and human analysts—to reason correctly about what is known versus inferred.

2. **Mathematically principled reconstruction**. Nuclear reconstruction is formulated as a confidence-weighted constraint optimization problem rather than a naïve inversion of degraded data. Constraints derived from Tier 1 measurements exert dominant influence, while Tier 2 and Tier 3 constraints contribute proportionally weaker guidance. This guarantees that reconstructed structures are maximally faithful to empirical ground truth wherever it exists, and explicitly underdetermined where it does not.

3. **Quantified uncertainty**. By generating ensembles of three-dimensional nuclear models, NucleoGenesis encodes uncertainty directly into the reconstructed state. Per-locus positional variance provides an explicit, spatially resolved measure of confidence, enabling downstream applications—such as simulation, hypothesis testing, or future physical instantiation—to discriminate between well-constrained and ambiguous regions of the nucleus.

4. **Future-proof system architecture**. The framework is designed for technological evolution rather than obsolescence. Version-controlled NBM evolution, deterministic artifact hashing, and explicit technology slots ensure that archived samples can be re-analyzed as new assays, sequencing chemistries, and reconstruction algorithms emerge. Information added in the future augments rather than invalidates prior reconstructions.

Critically, this work also draws a clear and principled boundary around what is *not* yet achievable. The transition from a digital nuclear blueprint to a functional physical nucleus remains a major unsolved challenge, requiring advances in gigabase-scale DNA synthesis, programmable chromatin assembly, and de novo nuclear envelope formation. These are not incremental engineering problems but paradigm-level gaps that may require decades of progress. NucleoGenesis does not collapse this distinction or make premature claims of physical realization.

Instead, it delivers the most complete, internally consistent digital nuclear representation that current science allows, while constructing an infrastructure explicitly designed to interface with future breakthroughs when—and if—they arrive.

Within this context, the strategic value of DBS archival becomes clear. A single DBS card archived today encodes biological identity in a form that is:

- Chemically stable across decades to centuries,
- Independent of cryogenic storage and continuous energy input,
- Compact and transportable across terrestrial or interplanetary distances,
- Re-analyzable using sequencing and reconstruction technologies not yet invented.

As humanity moves into environments where conventional biological preservation becomes fragile or impossible—deep-space missions, post-catastrophe recovery, or resource-constrained settings—DBS-based nuclear archiving offers a uniquely robust substrate for biological continuity. NucleoGenesis formalizes this substrate into a coherent scientific system, ensuring that biological information captured today remains interpretable, extensible, and actionable far into the future.

Final Perspective. NucleoGenesis does not attempt to outpace biology. Instead, it aligns with its constraints—chemical, physical, and temporal—while preserving maximal optionality for the future. By combining rigorous provenance, principled reconstruction, quantified uncertainty, and resilient archival, the framework reframes nuclear preservation not as an act of stasis, but as a long-term investment in biological memory. In doing so, it establishes a foundation upon which future generations may build capabilities that cannot yet be realized, without forfeiting the information required to do so.

A Mathematical Notation Summary

Symbol	Definition
$\mathcal{N}$	Nuclear Blueprint Manifest
$\mathcal{G}$	Genome layer (sequence + variants)
$\mathcal{M}$	Methylome layer (CpG methylation)
$\mathcal{C}$	Contact layer (Hi-C or imputed)
$\mathcal{X}$	Expression layer
$\mathcal{U}$	Uncertainty layer
τ	Confidence tier $\in \{1, 2, 3, 4\}$
$\mathcal{P}$	Provenance metadata
$\mathcal{E}$	Set of distance constraints
$\mathbf{X}$	3D coordinates $\in \mathbb{R}^{3\times N}$
$E(\mathbf{X})$	Total energy function
$\gamma(\tau)$	Tier penalty function
σ_i	Positional uncertainty of bead i
$\mathbf{R}$	Reconstruction readiness score
$H(\cdot)$	SHA-256 hash function

References

[1] Tavallaee, G. and Orouji, E. (2025). *Mapping the 3D genome architecture.* Computational and Structural Biotechnology Journal, 27:89–101.

[2] Han, J., Zhang, Z., and Wang, K. (2018). *3C and 3C-based techniques: the powerful tools for spatial genome organization deciphering.* Molecular Cytogenetics, 11(21).

[3] Zhou, T., Zhang, R., and Ma, J. (2021). *The 3D genome structure of single cells.* Annual Review of Biomedical Data Science, 4:21–41.

[4] Oluwadare, O., Highsmith, M., and Cheng, J. (2019). *An overview of methods for reconstructing 3-D chromosome and genome structures from Hi-C data.* Biological Procedures Online, 21(7).

[5] MacKay, K. and Kusalik, A. (2020). *Computational methods for predicting 3D genomic organization from high-resolution chromosome conformation capture data.* Briefings in Functional Genomics, 19(4):292–308.

[6] Hollegaard, M.V., Grauholm, J., Børglum, A., et al. (2009). *Genome-wide scans using archived neonatal dried blood spot samples.* BMC Genomics, 10:297.

[7] Fudenberg, G., Kelley, D.R., and Pollard, K.S. (2020). *Predicting 3D genome folding from DNA sequence with Akita.* Nature Methods, 17:1111–1117.

[8] Mirny, L.A. (2011). *The fractal globule as a model of chromatin architecture in the cell.* Chromosome Research, 19:37–51.

[9] Hutchison, C.A., et al. (2016). *Design and synthesis of a minimal bacterial genome.* Science, 351(6280):aad6253.

[10] Dekker, J., Alber, F., Aufmkolk, S., et al. (2023). *Spatial and temporal organization of the genome: Current state and future aims of the 4D nucleome project.* Molecular Cell, 83(15):2624–2640.

[11] Liu, T. and Wang, Z. (2018). *Reconstructing high-resolution chromosome three-dimensional structures by Hi-C complex networks.* BMC Bioinformatics, 19:496. `https://doi.org/10.1186/s12859-018-2464-z`

[12] Abbas, A., He, X., Niu, J., Zhou, B., Zhu, G., Ma, T., et al. (2019). *Integrating Hi-C and FISH data for modeling of the 3D organization of chromosomes.* Nature Communications, 10:2049. `https://doi.org/10.1038/s41467-019-10005-6`

[13] Ghosh, S.K. and Jost, D. (2018). *How epigenome drives chromatin folding and dynamics, insights from efficient coarse-grained models of chromosomes.* PLOS Computational Biology, 14(6):e1006159. `https://doi.org/10.1371/journal.pcbi.1006159`

[14] Esposito, A., Bianco, S., Fiorillo, L., Conte, M., et al. (2021). *Polymer models are a versatile tool to study chromatin 3D organization.* Biochemical Society Transactions, 49(4):1675–1684. `https://doi.org/10.1042/BST20201004`

[15] Nuebler, J., Fudenberg, G., Imakaev, M., Abdennur, N., and Mirny, L.A. (2018). *Chromatin organization by an interplay of loop extrusion and compartmental segregation.* Proceedings of the National Academy of Sciences, 115(29):E6697–E6706. `https://doi.org/10.1073/pnas.1717730115`

[16] Fudenberg, G., Imakaev, M., Lu, C., Goloborodko, A., Abdennur, N., and Mirny, L.A. (2016). *Formation of Chromosomal Domains by Loop Extrusion.* Cell Reports, 15(9):2038–2049. `https://doi.org/10.1016/j.celrep.2016.04.085`

[17] Falk, M., Feodorova, Y., Naumova, N., Imakaev, M., et al. (2019). *Heterochromatin drives compartmentalization of inverted and conventional nuclei.* Nature, 570(7761):395–399. `https://doi.org/10.1038/s41586-019-1275-3`

[18] Harris, H.L., Gu, H., Olshansky, M., Wang, A., Farabella, I., et al. (2023). *Chromatin alternates between A and B compartments at kilobase scale for subgenic organization.* Nature Communications, 14:2337. `https://doi.org/10.1038/s41467-023-38429-1`